GRADED INJECTION: A NEW APPROACH TO WIDE-BANDGAP LIGHT EMITTERS

Thesis by

Mark Phillips

In Partial Fulfillment of the Requirements

for the Degree of

Doctor of Philosophy

California Institute of Technology

Pasadena, California

1993

(Submitted May 19, 1993)

to b.

Acknowledgements

One of Tom McGill's most remarkable accomplishments is the group of people he has brought together to do research. I have been privileged to work with so many talented people—present and former students, staff and associates—that I can only begin to acknowledge them all.

I am particularly fortunate in the people I have worked with most closely in my research. Johanes Swenberg performed all of the optical experiments, as well as recent crystal growth and device fabrication. Mike Wang did the computer device modelling, maintained and operated the surface analysis chamber, installed and operated the X-ray diffractometer, and helped with the device fabrication. The technical contributions of J. O. McCaldin will be clear to anyone who reads this thesis; I greatly enjoyed his explanations of physical chemistry and the history of solid state device research. Tom himself worked tirelessly to provide the resources necessary for this work, and offered critical guidance and encouragement.

Yixin Liu contributed experimentally to the early stages of the light-emitter research, and also with a theoretical study of contacts to wide-bandgap materials. Brian Cole did the initial II-VI crystal growth and introduced me to the II-VI MBE machine. Doug Collins grew several III-V buffer layers for use as substrates for II-VI growth, and allowed me to use the III-V MBE machine without asking me to help maintain it. He also maintained the clean room and was an important source of advice on MBE growth and on the care and feeding of a Perkin-Elmer MBE system.

Richard Miles at Hughes Research Laboratories characterized several samples by X-ray diffraction. Andy Hunter and his group at Hughes Research Laboratories also characterized a number of Mg-alloys and N-doped samples. I believe this collaboration, with the encouragement and enthusiasm provided by O. J. Marsh of Hughes Carlsbad, will continue to be very productive.

Dave Chow was an important and generous source of information and advice, especially during the first two years of this research. Yasantha Rajakarunanayake contributed to the early stages of the II-VI light-emitter research, and also helped me get started on my first project with the group. I found my work with Ed Yu in his study of band offsets and interface reactions very rewarding, and this research provided information needed to design the graded-injection devices. Ed Croke frequently supplied UHV parts from his stock, and allowed me to borrow equipment in emergencies.

Ron Marquardt, Harold Levy, Yixin Liu, Shaun Kirby and Chris Springfield spent a great deal of time administering the group's computer resources; they, along with Rob Miles, Per-Olov Pettersson and Dave Reich, have made working in the McGill group very entertaining. Although I never worked directly with Mike Jackson, I wish his tenure in the group had overlapped more with mine.

Marcia Hudson deserves a great deal of credit for the rapid pace of this research. Her efficient administration of the group, assisted by Carol McCollum and Sandy Brooks, allowed me to spend a minimum amount of time on administrative detail.

I am very fortunate to have had Dave Ting as a colleague and a friend. He is an unusually practical and useful theorist; I suspect he was really supposed to do experiments.

Several people outside the McGill group have made my stay at Caltech more enjoyable. Kayoko Hirata is a delightful teacher, and her Japanese language course was interesting and challenging. Martin and Chris Bucher proved to be exceptionally entertaining housemates. My first office in the sub-basement of Bridge Laboratory would be an unpleasant memory if it were not where I met Jamil

Tahir-Kheli and Kathy Grzegorek.

Finally, I wish to thank my parents, Shirley and Oliver Phillips, for many years of encouragement and support.

List of Patents and Publications

A U.S. Patent Application for "WIDE BAND-GAP SEMICONDUCTOR LIGHT EMITTERS," covering the light emitter discussed in Chapter 3, has been filed by J. O. McCaldin, T. C. McGill and M. C. Phillips.

Work related to this thesis has been, or will be, published under the following titles:

n-CdSe/p-ZnTe based wide band gap light emitters: numerical simulation and design,
M. W. Wang, M. C. Phillips, J. F. Swenberg, E. T. Yu, J. O. McCaldin and T. C. McGill, *J. Appl. Phys.* **73**, 4660 (1993).

A new approach to wide band gap visible light emitters,
M. C. Phillips, J. F. Swenberg, M. W. Wang, J. O. McCaldin and T. C. McGill, *Physica B* **185**, 485 (1993).

Proposal and verification of a new visible light emitter based on wide band gap II-VI semiconductors,
M. C. Phillips, M. W. Wang, J. F. Swenberg, J. O. McCaldin and T. C. McGill, *Appl. Phys. Lett.* **61**, 1962 (1992).

Forming of Al-doped ZnTe epilayers grown by molecular beam epitaxy,
M. C. Phillips, J. F. Swenberg, Y. X. Liu, M. W. Wang, J. O. McCaldin and T. C. McGill, *J. Cryst. Growth* **117**, 1050 (1992).

Interfacial reactions and band offsets in the AlSb/GaSb/ZnTe material system,
E. T. Yu, M. C. Phillips, D. H. Chow, D. A. Collins, M. W. Wang, J. O. McCaldin and T. C. McGill, *Phys. Rev. B* **46**, 13379 (1992).

Measurement of the CdSe/ZnTe valence band offset by x-ray photoelectron spectroscopy,
E. T. Yu, M. C. Phillips, J. O. McCaldin and T. C. McGill, *J. Vac. Sci. Technol. B* **9**, 2233 (1991).

Characterization of CdSe/ZnTe heterojunctions,
M. C. Phillips, E. T. Yu, Y. Rajakarunanayake, J. O. McCaldin, D. A. Collins and T. C. McGill, *J. Cryst. Growth* **111**, 820 (1991).

Heterojunction approaches to light emitters: The role of band offsets,
E. T. Yu, Y. Rajakarunanayake, M. C. Phillips, J. O. McCaldin and T. C. McGill, *Extended Abstracts of the 22nd (1990 International) Conference on Solid State Devices and Materials, Sendai,* 601 (1990).

Growth and characterization of ZnSeTe epilayers and superlattices,
M. C. Phillips, Y. Rajakarunanayake, J. O. McCaldin, R. H. Miles, D. H. Chow, D. A. Collins and T. C. McGill, *Mat. Res. Soc. Symp. Proc.* **198**, 439 (1990).

Optical investigation of the band offset of $Cd_xZn_{1-x}Te/ZnTe$ and $ZnSe_xTe_{1-x}/ZnTe$ superlattices,

Y. Rajakarunanayake, M. C. Phillips, J. O. McCaldin, D. H. Chow, D. A. Collins and T. C. McGill, *Mat. Res. Soc. Symp. Proc.* **198**, 427 (1990).

Growth of ZnTe and $ZnSe_xTe_{1-x}$ epilayers and superlattices on GaSb,

M. C. Phillips, Y. Rajakarunanayake, J. O. McCaldin, D. H. Chow, D. A. Collins and T. C. McGill, *Proc. SPIE - Int. Soc. Opt. Eng.* **1285**, 152 (1990).

Band alignment of $Zn_{1-x}Cd_xTe/ZnTe$ and $ZnTe_{1-x}Se_x/ZnTe$ strained layer superlattices,

Y. Rajakarunanayake, M. C. Phillips, J. O. McCaldin, D. H. Chow, D. A. Collins and T. C. McGill, *Proc. SPIE - Int. Soc. Opt. Eng.* **1285**, 142 (1990).

Measurement of the valence band offset in novel heterojunction systems: Si/Ge (100) and AlSb/ZnTe (100),

E. T. Yu, E. T. Croke, D. H. Chow, D. A. Collins, M. C. Phillips, T. C. McGill J. O. McCaldin and R. H. Miles, *J. Vac. Sci. Technol. B* **8**, 908 (1990).

Abstract

In this thesis we propose a new device structure—the graded injector—for short-wavelength LEDs and laser diodes, and describe the growth, fabrication and characterization of green LEDs based on this structure. We also discuss the first growth by MBE of $Mg_xCd_{1-x}Se$ alloys, which are used for the graded injection region of the LEDs.

In spite of the important technological applications for short-wavelength LEDs and diode lasers, and in spite of over three decades of work on fabrication of light emitters from II-VI compounds, no II-VI LEDs or laser diodes are commercially available, and the demand for short-wavelength devices remains largely unfilled. This is due primarily to the difficulty of obtaining both p- and n-type doping in a II-VI with a bandgap large enough to emit green or blue light.

In recent years modern crystal growth techniques have contributed to substantial progress on—and a revival of interest in—II-VI compounds. This progress has occurred mainly on two fronts: metastable doping during low-temperature growth; and heterojunction approaches made possible by the increased control over the growth process afforded by new techniques such as MBE. We have pursued the latter approach, developing a novel heterojunction structure to avoid difficult doping.

In Chapter 1 we discuss applications of short-wavelength light emitters and the history of II-VI light emitter research, including current work by other groups. We examine the role of heterojunctions in LEDs and diode lasers in Chapter 2, and

graphically display theoretical and experimental values for band offsets among a variety of semiconductors using "McCaldin Diagrams." These diagrams help to clarify the problem, allow us to draw general conclusions about what we can and cannot hope to do, and lead to the device proposal of Chapter 3.

In Chapter 3 we first propose a new kind of heterojunction structure for wide-bandgap light emitters, then discuss the growth, fabrication and characterization of devices based on this proposal. The experiments demonstrate that the graded-$Mg_xCd_{1-x}Se$ structure allows injection of electrons into p-type ZnTe in spite of the unfavorable band offset between CdSe and ZnTe.

II-VI MBE has been studied much less than III-V MBE, and many aspects of the growth are different due to differences in the material systems. Furthermore, there had been little previous research on II-VI compounds containing Mg, and none using modern crystal growth techniques. Thus in Chapter 4 we discuss II-VI MBE and some of the difficulties encountered in growing graded-$Mg_xCd_{1-x}Se$ devices.

Contents

Acknowledgements iii

List of Patents and Publications vi

Abstract ix

List of Figures xiii

List of Tables xv

Glossary of Acronyms xvi

1 Introduction 1

1.1 Motivation 1

1.1.1 Light-emitting diodes 2

1.1.2 Diode lasers 9

1.2 Historical background 12

1.2.1 Growth 12

1.2.2 Doping 12

1.2.3 Molecular beam epitaxy 14

1.2.4 ZnSe 15

1.2.5 *p*-type doping of ZnSe 16

1.2.6 The heterojunction approach 20

1.3 The state of the art 20

1.3.1 ZnSe(N) 21
1.3.2 Graded $Mg_xCd_{1-x}Se$ 22
References 23

2 **Heterojunctions for Light Emitters** **29**
2.1 Introduction 29
2.2 McCaldin diagrams 32
2.3 n-CdSe/p-ZnTe 36
2.4 New material systems 39
References 42

3 **The Graded Injector** **44**
3.1 Proposal for a new light-emitting structure 44
3.2 Experiment 52
3.2.1 Graded-$Mg_xCd_{1-x}Se$ green LED 52
3.2.2 p-type doping of ZnTe 61
3.3 Conclusions 63
References 64

4 **MBE growth of II-VI Compounds** **65**
4.1 Introduction 65
4.2 Growth 65
4.2.1 Substrate choice 65
4.2.2 Substrate preparation and deoxidation 71
4.2.3 Substrate mounting for growth 72
References 74

List of Figures

1.1 Bandgap vs. lattice constant for III-V alloys 4
1.2 Relative luminosity function 6

2.1 Homojunction LED 30
2.2 Heterojunction LED 31
2.3 Example of an unfavorable heterojunction: n-ZnSe/p-ZnTe 33
2.4 McCaldin diagram for common semiconductors 35
2.5 n-AlSb/p-ZnTe heterojunction light emitter 37
2.6 n-CdSe/p-ZnTe heterojunction 38
2.7 McCaldin diagram including unusual II-VI compounds 41

3.1 Band profile in an abrupt n-CdSe/p-ZnTe heterojunction 45
3.2 Carrier densities in an abrupt n-CdSe/p-ZnTe heterojunction 46
3.3 McCaldin diagram with $Mg_xCd_{1-x}Se$ alloys. 47
3.4 Band diagrams of a graded-$Mg_xCd_{1-x}Se$ light emitter 49
3.5 Carrier densities in a biased graded-$Mg_xCd_{1-x}Se$ device. 50
3.6 Graded-$Mg_xCd_{1-x}Se$ blue LED 51
3.7 Graded-$Mg_xCd_{1-x}Se$ green LED structure 53
3.8 Mesa device structure 55
3.9 J-V of graded-$Mg_xCd_{1-x}Se$ green LED 57
3.10 Log J-V of graded-$Mg_xCd_{1-x}Se$ green LED 58
3.11 Comparison of J-V characteristics 59

3.12 Electroluminescence of a graded-$Mg_xCd_{1-x}Se$ LED 60
3.13 LED packaging 62

4.1 PL of ZnTe on ZnTe and GaAs 68
4.2 PL of ZnTe on ZnTe and GaSb 69

List of Tables

1.1 Characteristics of LED materials 3

Glossary of Acronyms

CW	continuous wave
DH	double heterojunction
IR	infrared
ITO	indium tin oxide
LED	light-emitting diode
LPE	liquid-phase epitaxy
MBE	molecular-beam epitaxy
MIS	metal-insulator-semiconductor
MOCVD	(=OMVPE=MOVPE) metalorganic chemical vapor deposition
MOMBE	metalorganic molecular-beam epitaxy
MOVPE	(=MOCVD=OMVPE) organometallic vapor-phase epitaxy
OMVPE	(=MOCVD=MOVPE) metalorganic vapor-phase epitaxy
PL	photoluminescence
RF	radio frequency
SH	single heterojunction
TEM	transmission electron microscopy
UHV	ultra-high vacuum
VPE	vapor-phase epitaxy
XPS	X-ray photoemission spectroscopy

Chapter 1

Introduction

1.1 Motivation

In the 25 years since the commercial introduction of LEDs for use as indicator lamps, improvements in brightness, efficiency, and lifetime have expanded the use of LEDs to a wide variety of displays and as light sources used in communications, printing, and copying; 1989 Japanese LED production alone was estimated at 5 billion units, worth 120 billion yen [1]. Diode laser applications have expanded beyond communications to optical memories, printers, and barcode scanners; 1992 worldwide production exceeded 49 million units, for sales of $287 million [2]. Considering these production volumes, it may be surprising to learn that the use of LEDs and diode lasers is limited by a lack of efficient blue LEDs and of commercial diode lasers operating at wavelengths shorter than red.

Section 1.1.1 describes the limitations of present commercial LED technology versus the potential applications for shorter-wavelength devices. Section 1.1.2 gives a similar discussion for diode lasers.

1.1.1 Light-emitting diodes

Current technology

Table 1.1 summarizes the materials used in visible LEDs, and gives typical performance characteristics for commercial devices made from these materials. The LEDs are arranged in order of decreasing wavelength. In general, the external quantum efficiency tends to decrease with decreasing wavelength, from as high as 21% in the red to 0.04% in the blue. This decrease in quantum efficiency with decreasing wavelength is the central weakness in current LED technology. It is the result of two problems which occur in wide-bandgap semiconductors: a trend towards indirect bandgaps in wider-bandgap III-V arsenides, phosphides and in SiC; and difficulties in doping to obtain *pn* junctions in most wide-bandgap semiconductors, including II-VIs and III-V nitrides [3].

Figure 1.1, a plot of bandgap versus lattice constant for the III-Vs which are presently most important for commercial LEDs, is useful for understanding Table 1.1. There are a variety of direct-bandgap compounds and alloys with bandgaps in the IR, particularly GaAs and $Al_xGa_{1-x}As$. Efficient IR laser diodes and LEDs based on these materials have reached a high state of technological development, but as we move to wider bandgaps the situation becomes less favorable. GaP, AlP, and AlAs all have indirect bandgaps, and the ternary alloys $GaAs_xP_{1-x}$ and $Al_xGa_{1-x}As$ become indirect in the red at 1.977 eV (627 nm) [5] and 1.90 eV (653 nm) [6], respectively.

The radiative efficiency of indirect-bandgap materials is so low that they would be useless as light-emitting materials were it not for "luminescence activators." These are impurities which create trapping centers in indirect-bandgap materials that allow momentum-conserving radiative recombinations without phonons. Simultaneous doping of GaP with Zn and O allows efficient donor-acceptor pair emission in the red, while isoelectronic N forms a shallow trap giving yellow-green emission in GaP, or emission at wavelengths from red to yellow in $GaAs_xP_{1-x}$ al-

Material: Light-emitting layer	Material: Substrate	Production method	Color	Wavelength (nm)	External quantum efficiency Max(%)	Luminous power efficiency (lm/W)	Axial luminous intensity (mcd)
GaP(Zn,O)	GaP	LPE	Red	700	2	1	30
$Al_{.35}Ga_{.65}As$	GaAs	LPE (SH)	Red	660	7	2.1	500
$Al_{.35}Ga_{.65}As$	AlGaAs	LPE (DH)	Red	660	21	12	5000
$GaAs_{.6}P_{.4}$	GaAs	VPE+diffusion	Red	660	0.15	0.07	20
$GaAs_{.45}P_{.55}$(N)	GaP	VPE+diffusion	Red	650	0.5	0.35	100
$GaAs_{.35}P_{.65}$(N)	GaP	VPE+diffusion	Red	630	0.65	1.2	300
$GaAs_{.25}P_{.75}$(N)	GaP	VPE+diffusion	Orange	610	0.6	2	300
$GaAs_{.15}P_{.85}$(N)	GaP	VPE+diffusion	Yellow	590	0.25	1.1	200
$GaAs_{.10}P_{.90}$(N)	GaP	VPE+diffusion	Yellow	583	0.2	1.1	200
GaP(N)	GaP	LPE	Yellow	570	0.7	4.3	400
GaP(N)	GaP	LPE	Yellow-green	560	0.3	1.6	250
GaP	GaP	LPE	Pure green	555	0.2	1.36	200
GaN*	α-Al_2O_3	VPE (MIS)	Blue	490	0.1	0.14	10(10mA)
SiC	SiC	LPE	Blue	480	0.04	0.04	12
ZnSe*	ZnSe	LPE+diffusion	Blue	480	0.03	—	2(2mA)
ZnS*	ZnS	MOCVD(MIS)	Blue	460	0.01	—	2(10mA)

Table 1.1: Typical performance characteristics of LED materials, as packaged for commercial use (except for the blue LEDs marked with an asterisk, which are not commercially available). Axial photometric values are for a 5ϕ package and 20 mA, unless otherwise indicated [1].

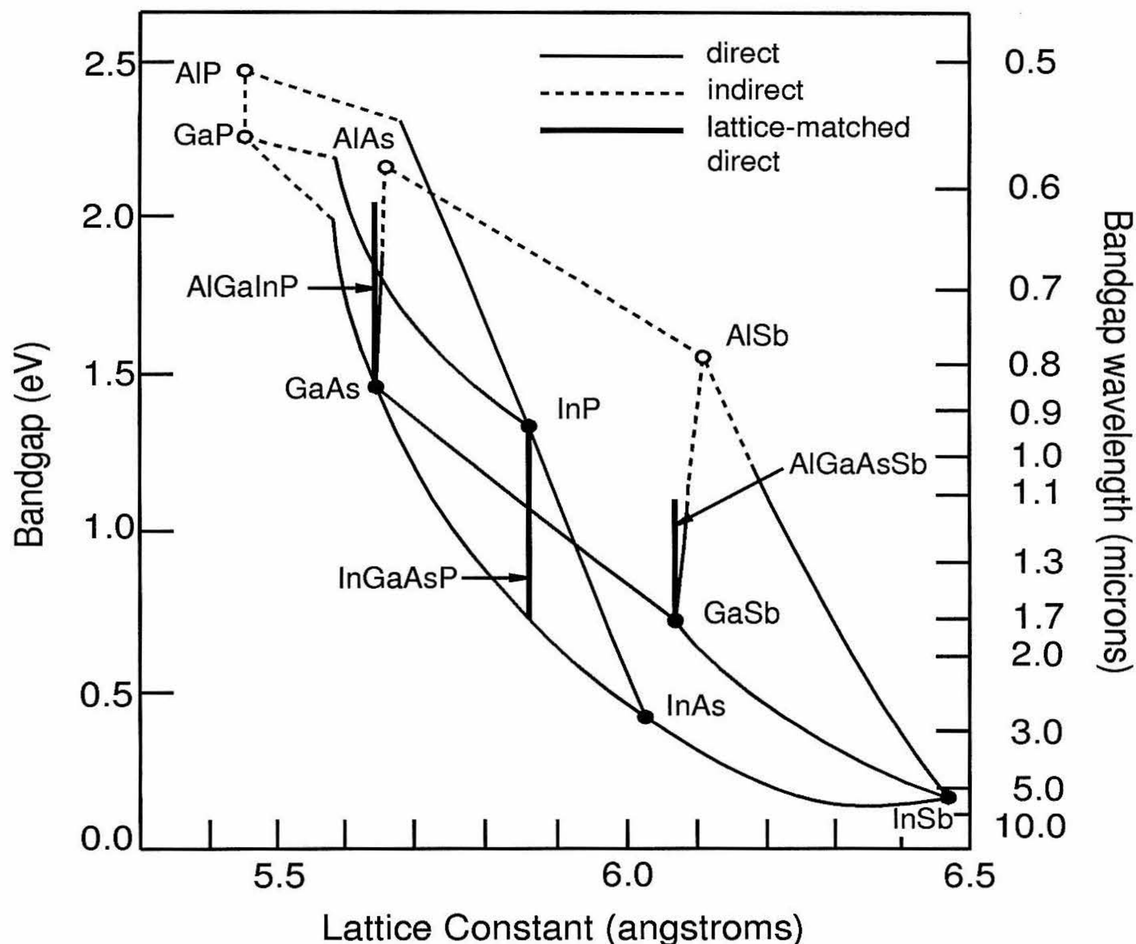

Figure 1.1: Bandgap versus lattice constant for the III-V binary compounds and alloys which are presently most important for commercial LEDs and diode lasers. Direct-bandgap compounds and alloys are represented by filled circles and solid lines. Indirect-bandgap compounds and alloys are plotted as open circles and dotted lines. Direct-bandgap quaternaries lattice-matched to convenient substrates are also indicated with heavy lines [4].

loys. Even with activators, luminescence in indirect-bandgap materials is far less efficient than in high-quality, direct-bandgap materials, but until quite recently there were no direct-bandgap alternatives for yellow and green devices which could beat GaP-based LEDs. In fact, GaP(N) is still the dominant technology for green LEDs. Even at red wavelengths, where $GaAs_xP_{1-x}$ and $Al_xGa_{1-x}As$ alloys have direct bandgaps, the availability of transparent substrates, growth techniques, and doping techniques favored indirect-bandgap GaP(Zn,O) or $GaAs_xP_{1-x}$(N) on GaP substrates for many years [7].

The $Al_xGa_{1-x}As$ LEDs listed in Table 1.1 are a more recent development, made possible by advances in $Al_xGa_{1-x}As$ technology for diode lasers. The best of these devices are double-heterojunction structures similar to laser diodes, and they are grown with a thick $Al_xGa_{1-x}As$ buffer to allow the absorbing GaAs substrates to be removed with a selective etch. These red LEDs are extremely efficient and spectacularly bright.

The close lattice match of $Al_xGa_{1-x}As$ over its entire composition range is crucial to the efficiency and reliability of high-brightness $Al_xGa_{1-x}As$ LEDs. The ternary alloys $In_xGa_{1-x}P$ and $Al_xIn_{1-x}P$ remain direct beyond the red, crossing over in the green around 2.239 eV (554 nm) and 2.33 eV (532 nm) [6], respectively, but the lattice mismatch in these systems is quite large. The only way to maintain lattice match is to work with quaternaries; the principal system of interest is $Al_xIn_yGa_{1-x-y}P$, which has a direct-to-indirect transition at 2.30 eV (539 nm) at room temperature for compositions lattice-matched to GaAs substrates [8]. Controlling the quaternary alloy concentration to maintain lattice match is a formidable challenge, but yellow devices which out-perform the orange and yellow devices listed in Table 1.1 by a factor of 10–20 have been reported by researchers at Hewlett-Packard [8], and are probably nearing commercial availability. These devices have external quantum efficiencies lower than the best red $Al_xGa_{1-x}As$ devices, but because the sensitivity of the human eye is much higher in the yellow than in the red (see Figure 1.2) these devices have a peak luminous

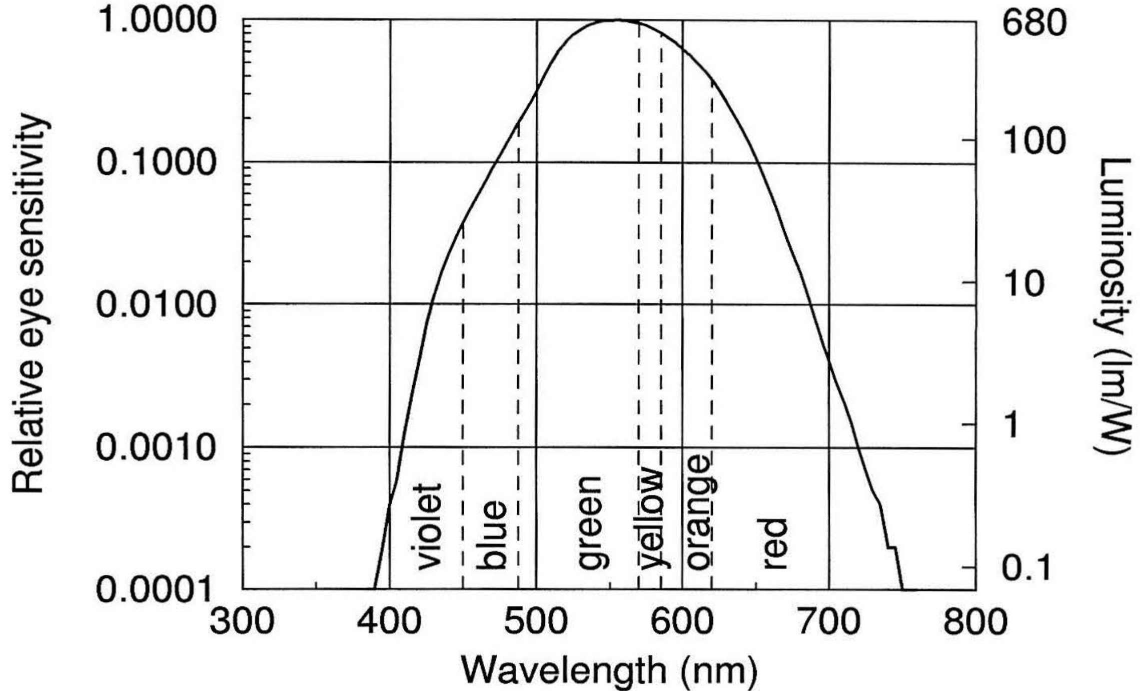

Figure 1.2: Relative luminosity function (sensitivity of the human eye vs. wavelength), V(λ), for normal, photopic vision [9].

efficiency of 20 lm/W, the highest ever reported for an LED.

In the yellow-green, GaP(N) LEDs have quantum efficiencies around 0.3%, and are only useful as indicators because the sensitivity of the human eye, as shown in Figure 1.2, peaks in the green at slightly shorter wavelengths. Though $Al_xIn_yGa_{1-x-y}P$ remains direct to 2.30 eV (539 nm) in the green, the researchers at Hewlett-Packard [8] reported that the radiative efficiency begins decreasing at 600 nm (2.07 eV). Thus the yellow-green LEDs reported by this group are only four times more efficient than existing GaP(N) devices.

The only commercial blue LEDs are made from SiC, a wide-bandgap semiconductor which occurs in more than 150 polytypes, at least some of which can be doped both p-type and n-type. Unfortunately, SiC has an indirect bandgap and the band structure is less amenable to the use of luminescence activators than

GaP [10]. The external quantum efficiency of the best SiC devices is almost a factor of ten less than that of yellow-green GaP(N) devices, and the sensitivity of the eye drops off rapidly at wavelengths shorter than green. Consequently SiC LEDs are only barely useful as indicators.

Alternatives to SiC include the direct-bandgap compounds GaN, AlN, ZnS, ZnSe, and $Mg_xZn_{1-x}Te$ alloys. ZnSe will be discussed in Sections 1.2 and 1.3; $Mg_xZn_{1-x}Te$ is one of the main topics of this thesis. ZnS is commonly used in phosphors, but has doping and material-quality problems similar to ZnSe, perhaps to an even more severe degree. ZnS received much attention in the 1960s and early 1970s, but ZnSe has been given more attention by researchers working with MBE in the 1980s and 1990s.

GaN and AlN have very large, direct bandgaps—3.39 eV [11] and 6.2 eV [12] at 300 K—but also have the growth and doping problems which generally accompany large bandgaps.[1] GaN tends to be heavily n-type, even when intentionally doped with acceptors, but recently Akasaki and coworkers [13] have used low-temperature growth and Mg doping to produce GaN with room-temperature free-hole concentrations of 4×10^{17} /cm^3. They have also fabricated blue LEDs with external quantum efficiencies of 0.8% and a luminous intensity of 150 mcd, substantially better than present commercial SiC LEDs. Very recently Moustakas [14] reported free-hole concentrations of up to 1×10^{19} /cm^3 in GaP(Mg) at 300K, but with no details of device performance. The major remaining problem with GaN is crystal quality, partly due to the unavailability of lattice-matched substrates. If the crystal-quality problems are solved, the nitrides may make good devices because they are very robust materials, but at present the growth technology is behind that of II-VI materials.

[1] So many problems, in fact, that George Craford, R&D Materials Manager at Hewlett-Packard Optoelectronics and a patriarch of LED technology, has suggested that GaN may actually be a II-VI compound.

Applications

LEDs were originally marketed as indicator lamps, and due to their low cost (average price < 20 ¢ apiece) and long lifetime, they are now ubiquitous in this application. As their brightness and efficiency have increased, they have been used in a variety of new applications. $Al_xGa_{1-x}As$ red LEDs are now bright enough to be visible in direct sunlight, and they are fifty times more efficient than a filtered incandescent bulb [15]. High-brightness $Al_xGa_{1-x}As$ LEDs are now commonly used as brake lights on automobiles, and may soon be used in traffic signals, where they provide a tenfold increase in lifetime [15].

The main limitation to the applications for LEDs is the lack of high-brightness LEDs at wavelengths shorter than red, and a lack of even moderately bright blue devices. High-brightness yellow $Al_xIn_yGa_{1-x-y}P$ LEDs are becoming available (see Section 1.1.1), and $Al_xIn_yGa_{1-x-y}P$ may provide better green devices as well, but it cannot provide the blue devices necessary for a full-color display. This will limit the use of LEDs in electronic displays, a growing market already several times larger than the current LED market.

Even without blue devices, the most important area of growth for LEDs in the next five years is expected to be large, outdoor, color displays [16]. The high efficiency and long lifetime of LEDs is very important in these applications; devices with lifetimes > 30000 hours are being developed for outdoor displays [17], which are already common in Japan, with the larger displays covering the sides of buildings.

LEDs are also displacing other light sources in many non-display applications. Yellow LEDs packaged on a bar with a reflector and a lens are being used as the light source for reading documents in facsimile machines. LEDs are displacing diode lasers in inexpensive "laser" printers. Shorter wavelengths are desirable for the light emitters used in laser printers and in color copiers because higher-energy photons greatly increase the photoconductivity, allowing the laser or LED to scan

much more quickly. If adequate blue LEDs were available, full-color images could be written onto color Polaroid film with LEDs to make inexpensive, full-color printers.

1.1.2 Diode lasers

Diode lasers are essentially a specialized form of LED, but the requirements for the material system are much more demanding. First, only direct-bandgap materials are efficient enough for practical diode lasers. For useful, room-temperature devices, the material system must be able to produce band offsets to confine carriers, and steps in the index of refraction to confine light. Finally, the band offsets and index steps must not create excessive lattice mismatch; generally lattice mismatch decreases efficiency and lifetime, though in some cases it is desirable to introduce small amounts of strain.

In general, the two degrees of freedom of a quaternary system are necessary to maintain lattice match while varying the bandgap. Controlling the alloy concentration of a quaternary is quite difficult, however, and the development of diode lasers would have been much more difficult had it not been for $Al_xGa_{1-x}As$. $Al_xGa_{1-x}As$ is a rare ternary material system in its ability to provide the appropriate band offsets and index steps while maintaining close lattice match.

To obtain wavelengths shorter than those accessible with $Al_xGa_{1-x}As$, commercial laser diode technology has been forced to move to the $Al_xIn_yGa_{1-x-y}P$ quaternary, but this has been a slow process. For even shorter wavelengths, a new material system must be developed to allow low-voltage minority-carrier injection, carrier confinement, optical confinement, and control of lattice match. Once such a material system is developed, the design of short-wavelength laser diodes will not be fundamentally different from the design of red and IR laser diodes. This thesis describes a material system and injection scheme for use in short-wavelength LEDs and laser diodes, but does not discuss the details of LED or diode laser design.

Current technology

The laser diode market, and hence laser diode technology, is divided into two distinct segments: visible and near-visible devices based on $Al_xGa_{1-x}As$ and related alloys, which are used in most applications other than communications; and longer-wavelength IR devices based on $In_xGa_{1-x}As$ and related alloys, which operate at wavelengths optimized for optical fiber communications. The communications market is quite large, but the non-communications market is now larger in sales (and overwhelmingly larger in units). The largest growth potential is in visible devices [18]. Since this thesis concerns a material system for short-wavelength devices, the longer-wavelength technology and market will be largely ignored in what follows.

Most non-communications applications benefit from the shortest possible wavelengths, and until very recently this meant devices fabricated from $Al_xGa_{1-x}As$. The direct-indirect crossover in $Al_xGa_{1-x}As$ occurs at about 653 nm, but fabricating devices close to this limit is difficult for a number of reasons. The easiest devices to fabricate operate at 800 nm [19], but the demand for shorter-wavelength devices has resulted in a gradual decrease in operating wavelength. The most common laser diodes—used in both compact disk players and laser printers—operate at 780 nm, but quite a few shorter-wavelength devices are now available.

To go to wavelengths shorter than the $Al_xGa_{1-x}As$ crossover, laser diode manufacturers have turned to the $Al_xIn_yGa_{1-x-y}P$ quaternary system. This is the material system which is being used for high-brightness yellow LEDs (see Section 1.1.1), but because of the added difficulties of making laser diodes, it is presently being used for red lasers around 630 nm. Manufacturers are working on devices operating at shorter wavelengths, but higher Al concentrations tend to shorten device lifetime [19].

Before the announcement of ZnSe(N) blue-green laser diodes (which will be discussed in detail in Sections 1.3.1 and 1.2.5) the shortest wavelength diode

lasers were research devices based on $Al_xIn_yGa_{1-x-y}P$, operating in the yellow at 584 nm [20]. In spite of elaborate heat sinking, including mounting on diamond, these devices operated CW at 77 for only a very short time. This alloy system may eventually be the basis for yellow, or possibly green, commercial laser diodes, but not for blue lasers.

Applications

Laser diodes accounted for about 23% of the $1.074 billion world laser market in 1991 [21], corresponding to 99.9% of sales by unit. Market projections for 1992 estimated that 4×10^7 laser diodes would be used in optical memories (including compact disk players), and 7×10^6 in laser printers. Shorter wavelengths are desirable in both of these applications. The wavelength of the laser reading the information from an optical disk determines the maximum storage density, hence a factor of two decrease in wavelength from IR to blue increases the maximum storage density by a factor of four. Shorter wavelengths in laser printers increase resolution and increase the printing speed by enhancing photoconductivity. There are a variety of other applications such as bar code scanning, alignment and control, and full-color displays which also benefit from or require shorter wavelengths.

Accurately predicting the potential market for short-wavelength laser diodes is quite difficult. At high unit prices, green or blue laser diodes would begin to replace more expensive ion or solid state lasers, just as 780 nm laser diodes replaced He-Ne lasers in printers. One estimate suggests there would be demand for 1000 blue laser diodes per year if they were available at $1000 apiece [22]. At lower unit prices they would begin to displace most of the red laser diodes in optical memories and printers. Substantial demand might come from applications which are simply not cost effective with expensive ion or solid state lasers. Regardless of the exact numbers, it is not difficult to understand the motivation for the intense research presently directed at short-wavelength LEDs and laser diodes.

1.2 Historical background

In the introduction to his review, "Current approaches to *pn* junctions in wider bandgap II-VI semiconductors," McCaldin [23] gives a brief overview of the history of research on II-VI semiconductors. He points out that Zn chalcogenides had been used as phosphors for decades before the first *pn* junctions were made, yet they were left behind in the semiconductor revolution started by devices made from Ge and Si. Even as efficient III-V LEDs and diode lasers were being developed, and even though the large, direct bandgaps of the Zn chalcogenides made them obvious choices for short-wavelength devices, no commercially successful II-VI LEDs or diode lasers were developed, and none are available today.

1.2.1 Growth

The first problem with II-VIs was that conventional bulk growth techniques such as melt growth, which works well for Ge and Si, or vapor growth near thermal equilibrium, generally do not produce high-quality II-VIs. At the high temperatures required for these techniques it is difficult to prevent contamination from impurities in the crucibles or ampoules used to contain the growth, and the high vapor pressures of the constituents makes control of stoichiometry difficult [24]. Modern, low-temperature crystal growth techniques such as MOCVD and MBE can produce high-quality epitaxial layers of II-VIs, but the difficulty of bulk growth remains a problem for substrates—most II-VI epilayers are grown on III-V substrates because II-VI substrates are usually small, expensive, difficult to obtain, and of poor structural quality.

1.2.2 Doping

The second problem encountered with II-VIs was doping, and this difficulty has proved much more intractable. Using conventional doping techniques (*i.e.*, exclud-

ing the use of Li or the metastable doping techniques discussed below) binary II-VI compounds with bandgaps larger than that of CdTe can be doped either *p*-type or *n*-type, but not both: tellurides tend to be *p*-type, the rest *n*-type. This means that the most basic LED device structure—the *pn* homojunction—is very difficult to obtain with II-VIs. Many of the prototype II-VI LEDs reported in the literature have been MIS structures [25], but none of these structures proved efficient enough to be commercially successful. In fact, all commercial LEDs and diode lasers are based on *pn* junctions, and most wide-bandgap II-VI research has centered on understanding and solving—or at least solving—the doping problem.

McCaldin points out in his review [23] that the doping problem is not the result of a lack of shallow dopants, but rather arises from compensating charges which appear whenever dopants are introduced in an attempt to obtain the difficult doping type, *e.g.*, *p*-type in ZnSe. The observation that doping both *p*-type and *n*-type is difficult in most other large bandgap semiconductors suggests that the large bandgaps themselves may be part of the problem. The simple explanation for the case of ZnSe is that a Se vacancy is a double donor, thus creating one Se vacancy in an *n*-type ZnSe crystal allows two electron-hole recombinations, each releasing roughly the energy of the bandgap. If this energy exceeds the energy required to form the Se vacancy, then the self-compensated state is energetically preferable. Unfortunately the thermochemistry of ionizable defects which developed along these lines [26] predicted different defect species than those found in the detailed photoluminescence studies of Dean [27]. These studies found compensation by trace impurities, but subsequent improvements in purity have not solved the doping problems, perhaps because compensation by native defects takes over as trace impurities are removed.

1.2.3 Molecular beam epitaxy

After a period of intense research on II-VIs during the 1960s, interest waned in the 1970s, probably because little progress was being made on the doping problems. At the same time, new growth techniques which would eventually renew interest in wide-bandgap II-VIs were being developed using other material systems. Though some of the early work which led to the development of MBE was done with Pb chalcogenides [28], after the work on III-V compounds by Cho and Arthur [29] around 1970, almost all MBE research concentrated on III-V compounds for several years. In 1975 Smith and Pickhardt [30] reported the growth of Zn and Cd selenides and tellurides by MBE, and in 1976 Yao [31, 32] published the first of a series of studies on MBE growth of Zn chalcogenides. Still, very few MBE machines were dedicated to wide-bandgap II-VI materials until the late 1980s, possibly because of the high cost of the equipment and the difficulty of using a chamber for any other material once it has been used with II-VI compounds.

MBE has a number of advantages for the growth of II-VI compounds. Growth temperatures are much lower than for bulk growth processes, *e.g.*, as low as 200 °C for MBE of ZnSe, compared to over 1520 °C for melt growth. The source material, either elements or compounds, can be obtained in 99.9999% purity or better, and the entire process is performed in UHV. This produces layers of very high purity—PL spectra of undoped epilayers grown by MBE are often dominated by free-exciton emission. Low-temperature growth also avoids non-stoichiometric defects such as precipitates, which frequently occur in bulk growth of II-VIs, and allows heteroepitaxial growth on substrates such as GaAs and GaSb, which are available in large sizes and high quality. At MBE growth temperatures, interdiffusion or reaction between III-V substrates and II-VI epilayers can often be limited to a few atomic layers; bulk growth temperatures exceed the melting point of most III-V substrates.

Modern, low-temperature, epitaxial growth techniques such as MOCVD and

MBE have successfully solved most of the crystal growth problems which faced earlier II-VI researchers, but initial expectations that low-temperature growth alone would also solve the doping problems [24] have been disappointed. These expectations were based on the argument that if a crystal is doped during growth at a temperature low enough that there is not enough thermal energy available to overcome the activation energy for the formation of compensating defects, then the crystal might remain in the metastable uncompensated state. Unfortunately this technique has not worked well. For instance, both Cl and Al are shallow donors in ZnTe with binding energies, measured in luminescence experiments [33], of 20.1 meV and 18.3 meV, respectively. However, neither dopant produces n-type conductivity when incorporated during bulk growth or by diffusion, and the compensation mechanism for the case of Al—wherein Al donors are compensated by an acceptor complex consisting of an Al atom and a Zn vacancy—was studied in detail in the 1960s [34]. Since Al is known to be a shallow donor, and since the compensation by Zn vacancies is well established, ZnTe(Al) seems to be a promising candidate for metastable doping during low-temperature MBE, but growth at temperatures as low as 270 °C produces very high-resistivity material [35]. Similarly, Cl doping during MBE growth of ZnTe also produces high-resistivity material [36].

1.2.4 ZnSe

ZnSe/GaAs

Though Yao and other early researchers who studied MBE of wide-bandgap II-VIs did not find a solution to the doping problems, the improvements in material quality were impressive enough to attract new researchers and funding to the field. During the 1980s a number of groups set up wide-bandgap II-VI MBE efforts, most of them working on material systems related to ZnSe/GaAs. This system was deemed particularly interesting for several reasons. First, the bandgap of ZnSe (2.67 eV at 300 K) is in the blue. Second, ZnSe lattice-matches to GaAs

to within 0.26%, allowing the use of relatively large, high-quality, and inexpensive GaAs substrates. The conduction band offset between GaAs and ZnSe also allows injection of electrons from n-type GaAs to n-type ZnSe, thus back contacts can be made to the substrate for electrical devices. The importance of the availability of substrates, and of standardized procedures for cleaning, etching, bonding and deoxidizing these substrates for MBE growth, should not be underestimated; it undoubtedly influenced many researchers to work with ZnSe.

A large body of research developed concerning growth of ZnSe on GaAs: studies of the ZnSe/GaAs interface by TEM, XPS and electrical measurements; X-ray and TEM studies of misfit dislocations in thick ZnSe epilayers on GaAs; studies of out-diffusion of atoms from the GaAs during growth of the ZnSe; improvements in n-type doping; and studies of various quantum well or superlattice structures in ZnSe epilayers. The justification for most of this research was that it would be useful in wide-bandgap light emitters if ZnSe could be doped p-type.

1.2.5 p-type doping of ZnSe

The column V elements Sb, As, P and N, the column I elements Na and Li, and the isoelectronic impurity O, have all been incorporated as potential p-type dopants in ZnSe during various bulk and thin film growth processes, or by diffusion or ion implantation afterwards [37, 38, 39, 40]. As, P, N, Na and Li produce shallow acceptor levels when incorporated in small concentrations; there has been at least one report that Sb does not [37]. The p-type conductivity which is associated with O doping is difficult to understand, since isoelectronic O should be a donor. As, P, N, Na, and Li produce qualitatively similar results: small concentrations produce a shallow acceptor state, but as more of the dopant is incorporated, deep levels are also produced. For example, P produces a shallow acceptor with a binding energy of 80-92 meV when incorporated in low concentrations (perhaps a few$\times 10^{15}$ /cm^3 or less), but then at higher concentrations begins to introduce deep levels 0.6–0.7

eV above the valence band edge [38, 41]. The dopant concentrations at which deep levels dominate the electrical behavior depend on the dopant, the doping technique, and the crystal growth technique. Only Li and N have given significant and reproducible levels of *p*-type conductivity; As, P and Na generally have not produced measurable *p*-type conductivity; Akimoto *et al.* [40] induced *p*-type conductivity with O, but only to estimated carrier concentrations of 1.2×10^{16} /cm^3.

ZnSe(Li)

The first report of *p*-type conductivity in ZnSe grown by MBE was made in 1988 by Cheng *et al.* at 3M [42]. By doping with Li during growth they were able to achieve net acceptor densities of 1×10^{17} /cm^3 [43] and resistivities below 3 Ω cm. There had been previous reports of *p*-type ZnSe grown by other techniques [44], and the carrier concentrations were still two orders of magnitude too low for a good ohmic contact [45], but this was high-quality material with a resistivity low enough for the *p*-type region of a device, and it generated a great deal of enthusiasm about *p*-type ZnSe.

Aside from the saturation of the net acceptor concentration at 1×10^{17} /cm^3 and the consequent ohmic contacting problems, Li is a very undesirable dopant because of its diffusivity. Residual Li in Si devices causes serious problems due to the drift in device parameters caused by electromigration. Ge(Li) particle detectors are generally stored in a freezer to slow down the Li diffusion. Li can incorporate either substitutionally or interstitially, and can switch between the two depending upon Fermi level and temperature; researchers at Grenoble [46] performed extensive research on the complex behavior of Li in ZnTe. Though there were suggestions that Li does not move in ZnSe at room temperature (certainly the diffusivity is much lower than in Si or Ge [23]), or that when it does electromigrate it is actually beneficial [47], few researchers seem to regret the eclipse of Li doping by N doping.

ZnSe(N) and the first II-VI laser diode

Since all of the shallow acceptors which had been identified in ZnSe showed similar tendencies to generate compensating levels, researchers looked for a combination of dopant, doping technique and growth technique which could suppress the self-compensation and give the maximum net acceptor concentration. Researchers using MBE generally tried first those dopants which could easily be evaporated from an effusion cell; of these, only Li produced substantial *p*-type conductivity.

N is a particularly difficult dopant to incorporate during MBE growth because the N_2 molecule is very tightly bound. At growth temperatures around 300 °C it is extremely improbable that an N_2 molecule will find enough thermal energy to dissociate and allow the N to substitute on a Se site. Early work on N doping was done by doping with NH_3 during LPE or MOCVD [48], or by ion implantation after growth [49]. Both groups identified a shallow acceptor in the luminescence spectra, but the MOCVD material remained *n*-type due to residual donors, and the ion implanted material was *p*-type with a resistivity of 10^5 Ω cm due to damage from the high-energy implantation process. Park *et al.* [50] also identified a shallow acceptor resulting from small amounts of N incorporated during MBE growth with a large overpressure of N_2 or NH_3.

In 1990, Taike *et al.* [51] reported a hole concentration of 5.6×10^{17} /cm^3 in ZnSe grown by MOMBE using NH_3 as a doping source. This improved the best previous results by more than one order of magnitude, but there have since been questions about the reproducibility of this result. At an MBE conference in 1990, Ohkawa *et al.* [52] announced *p*-type conductivity in ZnSe doped with N from a plasma source during MBE. Almost simultaneously, Park *et al.* [53] reported hole concentrations of 3.4×10^{17} /cm^3 in ZnSe(N) grown by the same method but with a slightly different plasma source. These results were not only repeatable, but improvable: several groups using the same technique have reported hole concentrations around 1×10^{18} /cm^3 [54].

The N plasma doping source replaces one of the effusion cells on an MBE machine. An RF plasma is struck in a small chamber fed with high-purity nitrogen through a leak valve. At one end of the chamber confining the plasma, a plate with small orifices allows some of the plasma to escape and impinge on the substrate during growth. The simplest model of the doping process is that some of the molecules dissociate in the plasma so that N atoms or ionized atoms arrive at the growing ZnSe and incorporate substitutionally on a Se site. The fraction of molecules which dissociate is very small, however, so most of the flux is made up of various excited states of N_2 molecules. Ions which have been accelerated in the plasma, and various excited states of N_2 molecules, interact with the growing crystal in complicated ways. In short, the doping process is poorly understood; even the species responsible for the doping is a subject of debate [55].

ZnSe can be doped with a N plasma source to resistivities below 1 Ω cm, which is adequate for the bulk *p*-type region of a laser diode, but the corresponding net acceptor concentration is at least an order of magnitude too low for an adequate ohmic contact [45]. Forward biasing the *pn* junction requires avalanching the Schottky barrier to the *p* region, so that several volts are lost at the contact. Biasing to typical laser diode current densities required over 20 V in most of the ZnSe *pn* junctions being grown in 1990; a diode laser based on these *pn* junctions would have to dissipate a large amount of power. Furthermore there was no lattice-matched, double-heterojunction laser structure which could be grown with ternary alloys of ZnSe [56]. Any laser structure would have high misfit-dislocation densities due to the lattice mismatch. Thus many researchers were surprised when Haase *et al.* [57] at 3M announced the first blue-green laser diodes in 1991. These devices operated only at low temperatures and had to be pulsed to allow heat to dissipate, but their 490 nm emission was a remarkable improvement over all previous laser diodes.

1.2.6 The heterojunction approach

MBE offers not only improved crystal quality and low-temperature growth, but also vastly improved control of layer thicknesses and compositional changes. The ability to make atomically abrupt changes in composition opens up a variety of device structures which were unthinkable with bulk crystal growth techniques. Instead of struggling with doping to obtain a *pn* homojunction, the *p*-type and *n*-type regions can be different materials—two II-VIs, or even a III-V and a II-VI–forming a *pn* heterojunction.

Heterojunctions are not, however, a panacea; lattice match, band alignment and interface reactions must be carefully considered. The discussion of heterojunctions in Chapter 2 will show that there are very few candidates for simple *pn*-heterojunction wide-bandgap light emitters, and considerations of lattice match and band alignment led to the more complicated heterojunction device described in this thesis.

1.3 The state of the art

Research on wide-bandgap II-VI light emitters is presently following two distinct paths. The majority of II-VI researchers were working on ZnSe-based systems before the successes with ZnSe laser diodes at 3M. Since those successes, a number of other groups have entered the field, and nearly all of them are working on N-doped ZnSe devices very similar to the 3M devices. This is the most advanced technology at present, but problems with device lifetime and contacting have proved to be very difficult.

We have been pursuing a different approach, one which employs heterojunctions to avoid metastable doping. Since the metastable doping is itself the source of at least the contacting problems in the ZnSe devices, if not also the device lifetime problems, the heterojunction approach may be the better solution.

1.3.1 ZnSe(N)

Since the initial announcement of blue-green laser diodes by 3M in 1991, a number of other groups have reported lasing in similar structures, but the operating characteristics of 3M's devices have generally been substantially better than those reported by any other group. The most recent reports from 3M are probably the best gauge of the state of the art of ZnSe(N) lasers.

The threshold voltage of 3M's lasers has dropped from 15–20 V in the first structures reported, to 9 V in the most recent [58]. The initial devices operated pulsed at low temperatures; the present devices operate CW at 80K and pulsed at 300K. Most of this improvement is due to an improved contact formed by growing the last layer of ZnSe under the Au contact at 150 °C, which increases the net acceptor concentration to 2×10^{18} /cm^3 at the cost of a reduction in crystal quality. Threshold current densities at 80K have dropped from 320 A/cm^2 to 95 A/cm^2, mostly as the result of adding dielectric coatings to the facets. They have also fabricated index guided structures to obtain a single, transverse mode.

On the other hand, very little progress has been made on understanding or improving the N plasma doping process. The maximum net acceptor concentration has remained around 1–2×10^{18} /cm^3, and though several "improved" contacts have been reported [59, 60], none has produced a laser with characteristics superior to the 3M devices with Au/ZnSe contacts. Perhaps more serious are the short device lifetimes. The best devices last about one hour CW at 80K or pulsed at 300K. The heat produced by the voltage at the contact is probably responsible for some of these problems, but studies by 3M on ZnSe(N) LEDs have shown degradation even during low-current operation. The mechanism for the degradation is not known, but relaxation of the metastable N doping or problems resulting from misfit dislocations are leading candidates.

The misfit dislocation density in the ZnSe(N) laser structures is usually around 10^7/cm^2. 6–7% S is added to the ZnSe to form optical cladding layers, since this

ZnS_xSe_{1-x} alloy lattice matches to the GaAs substrates. Alloying with this amount of S produces a very small index difference so that the ZnSe guiding layer must be over the critical thickness for ZnSe on GaAs. Increasing the S concentration in the cladding layers to provide more index difference would enhance the mismatch. One possible solution to this problem has been reported by a group at Sony working with $Mg_xZn_{1-x}S_ySe_{1-y}$ alloys lattice-matched to GaAs [61]. These alloys can provide a large index difference while maintaining lattice match, and can also be used to open up the bandgap to give shorter-wavelength emission. Using this material system the Sony group has reported the first truly blue laser diodes, emitting at 447 nm, though operating only at 77 K [62]. Controlling the alloy concentration of this quaternary to obtain lattice match is particularly difficult.

1.3.2 Graded $Mg_xCd_{1-x}Se$

All II-VI laser diodes which have been reported to date are based on ZnSe and alloys of ZnSe grown by MBE and doped with a N plasma. The graded $Mg_xCd_{1-x}Se$ devices discussed in this thesis are one of the few II-VI-based alternatives to the ZnSe(N) technology. The $Mg_xCd_{1-x}Se$ devices are still at an earlier stage of development—at present, only green LEDs have been demonstrated—but they may provide the alternative to ZnSe(N) devices if the lifetime and contacting problems remain unsolved.

Bibliography

[1] M. Watanabe, *J. Electronic Engineering* suppl. (1), 37 (1990).

[2] M. Levitt, *Proc. SPIE - Int. Soc. Opt. Eng.* **1719**, 1 (1992).

[3] For the basic physics of LEDs—including a discussion of direct and indirect bandgaps—see Chapter 12 of Sze [9]; for a detailed discussion, see Casey and Panish [5].

[4] After S. Dokras, *Proc. SPIE - Int. Soc. Opt. Eng.* **1315**, 91 (1990); crossover points and $Al_xIn_{1-x}P$ bandgap data from Casey and Panish [5, 6].

[5] H. C. Casey, Jr. and M. B. Panish, *Heterostructure Lasers: Part A, Fundamental Principles* (Academic Press, New York, 1978), pp. 188–194.

[6] H. C. Casey, Jr. and M. B. Panish, *Heterostructure Lasers: Part B, Materials and Operating Characteristics* (Academic Press, New York, 1978), pp. 14–24.

[7] For the history of LED development, see A. A. Bergh and P. J. Dean, *Light-Emitting Diodes* (Clarendon Press, Oxford, 1976).

[8] K. H. Huang, J. G. Yu, R. M. Fletcher, T. D. Osentowski, L. J. Stinson, M. G. Craford and A. S. H. Liao, *Appl. Phys. Lett.* **61**, 1045 (1992).

[9] After S. M. Sze, *Physics of Semiconductor Devices* (John Wiley & Sons, New York, 1981), p. 689; CIE data from G. Wyszecki in *Handbook of Optics*, edited by W. Driscoll and W. Vaughan (McGraw-Hill, New York, 1978).

[10] Bergh and Dean [7], p. 70.

[11] H. Amano, M. Kitoh, K. Hiramatsu and I. Akasaki, *Jpn. J. Appl. Phys.* **28**, L2112 (1989).

[12] P. B. Perry and R. F. Rutz, *Appl. Phys. Lett.* **33**, 319 (1978).

[13] I. Akasaki, N. Koide, K. Manabe and H. Amano, presented at the 7th Trieste Semiconductor Symposium on Wide-Band-Gap Semiconductors, June 8-12, 1992, Trieste, to be published in *Physica B* (1993).

[14] D. Moustakas, *Bull. Am. Phys. Soc.* **38**, 445 (1993).

[15] S. Koike and I. Teramoto, *Oyo Buturi* **53**, 132 (1984).

[16] B. Roth, *OE Rep.*, April 1992, p. 4.

[17] Y. Idei, *Display Device* **5**, 38 (1992).

[18] D. Kales, *Laser Focus World* **28**, 56 (1992).

[19] G. T. Forrest, *Proc. SPIE - Int. Soc. Opt. Eng.* **1520**, 37 (1991).

[20] I. Hino, S. Kawata, A. Gomyo, K. Kobayashi, and T. Suzuki, *Appl. Phys. Lett.* **48**, 557 (1986).

[21] Laser market data in this section is from Forrest [19], unless otherwise noted.

[22] G. T. Forrest, *OE Rep.*, October 1990, p. 6.

[23] J. O. McCaldin, *J. Vac. Sci. Technol. A* **8**, 1188 (1990).

[24] T. Yao in *The Technology and Physics of Molecular Beam Epitaxy,* edited by E. H. C. Parker (Plenum, New York, 1985).

[25] See, for example, J. Gu, K. Tonomura, N. Yoshikawa and T. Sakaguchi, *J. Appl. Phys.* **44**, 4692 (1973); J.-L. Tissot, G. Labrunie and J. Marine, *IEEE*

Electron Device Lett. **ED-26**, 1202 (1979); or P. C. Eastman, R. R. Haering and P. A. Barnes, *Solid–State Electron.* **7**, 879 (1964).

[26] F. A. Kroger, *J. Phys. Chem. Solids* **26**, 1717 (1965).

[27] P. J. Dean, *J. Luminescence* **18/19**, 755 (1979).

[28] J. N. Zemel, J. D. Jensen and R. B. Schoolar, *Phys. Rev.* **140** A, 330 (1965).

[29] For a review of the development of MBE, see A. Y. Cho and J. R. Arthur, *Prog. Solid State Chem.* **10**, 157 (1975).

[30] D. L. Smith and V. Y. Pickhardt, *J. Appl. Phys.* **46**, 2366 (1975).

[31] T. Yao, S. Amano, Y. Makita and S. Maekawa, *Jpn. J. Appl. Phys.* **15**, 1001 (1976).

[32] See Yao [24] for a review of MBE of II-VI compounds.

[33] J. L. Pautrat, J. M. Francou, N. Magnea, E. Molva and K. Saminadayar, *J. Cryst. Growth* **72**, 194 (1985).

[34] R.S. Title in *Physics and Chemistry of II-VI Compounds,* edited by M. Aven and J. S. Prener (Elsevier, New York, 1967).

[35] M. C. Phillips, J. F. Swenberg, Y. X. Liu, M. W. Wang, J. O. McCaldin and T. C. McGill, *J. Cryst. Growth* **117**, 1050 (1992).

[36] Y. Hishida, T. Toda and T. Yamaguchi, *J. Cryst. Growth* **117**, 396 (1992).

[37] R. M. Park, J. Kleiman, H. A. Mar and T. L. Smith, *J. Appl. Phys.* **63**, 2851 (1988).

[38] T. Yao and Y. Okada, *Jpn. J. Appl. Phys.* **25**, 821 (1986).

[39] R. N. Bhargava, *J. Cryst. Growth* **59**, 15 (1982).

[40] K. Akimoto, T. Miyajima and Y. Mori, *Jpn. J. Appl. Phys.* **28**, L531 (1989).

[41] J. M. DePuydt, T. L. Smith, J. E. Potts, H. Cheng and S. K. Mohapatra, *J. Cryst. Growth* **86**, 318 (1988).

[42] H. Cheng, J. M. DePuydt, J. E. Potts and T. L. Smith, *Appl. Phys. Lett.* **52**, 147 (1988).

[43] J. Qiu, J. M. DePuydt, H. Cheng and M. A. Haase, *Appl. Phys. Lett.* **59**, 2992 (1991).

[44] For a review of doping in ZnSe before 1982, see Bhargava [39]. For a review of p-type ZnSe from 1982 to 1989, see McCaldin [23].

[45] For a discussion of ohmic contacts, see E. H. Rhoderick and R. H. Williams, *Metal-Semiconductor Contacts* (Clarendon Press, Oxford, 1988).

[46] See, for example, B. Benshel and M. Dupuy, *Phys. Stat. Solid.* **56**, 99 (1979).

[47] M. A. Haase, J. M. DePuydt, H. Cheng and J. E. Potts, *Appl. Phys. Lett.* **58**, 1173 (1991).

[48] P. J. Dean, W. Stutius, G. F. Neumark, B. J. Fitzpatrick and R. N. Bhargava, *Phys. Rev. B* **27**, 2419 (1983).

[49] Z. L. Wu, J. L. Merz, C. J. Werkhoven, B. J. Fitzpatrick and R. N. Bhargava, *Appl. Phys. Lett.* **40**, 345 (1982).

[50] R. M. Park, H. A. Mar and N. M. Salansky, *J. Appl. Phys.* **58**, 1047 (1985).

[51] A. Taike, M. Migita and H. Yamamoto, *Appl. Phys. Lett.* **56**, 1989 (1990).

[52] K. Ohkawa, T. Karasawa and T. Mitsuyu, *J. Cryst. Growth* **111**, 797 (1991).

[53] R. M. Park, M. B. Troffer, C. M. Rouleau, J. M. Depuydt and M. A. Haase, *Appl. Phys. Lett.* **57**, 2127 (1990).

[54] See, for example, R. M. Park, M. B. Troffer, E. Yablonovitch and T. J. Gmitter, *Appl. Phys. Lett.* **59**, 1896 (1991); or Z. Yang, K. A. Bowers, J. Ren, Y. Lansari, J. W. Cook, Jr. and J. F. Schetzina, *Appl. Phys. Lett.* **61**, 2671 (1992); or Qiu *et al.* [43].

[55] Compare, for example, Park *et al.* [53] and K. Ohkawa, A. Tsujimura, S. Hayashi, S. Yoshii and T. Mitsuyu, presented at the 7th Trieste Semiconductor Symposium on Wide-Band-Gap Semiconductors, June 8-12, 1992, Trieste, to be published in *Physica B* (1993).

[56] For the physics of laser diodes—including single- and double-heterojunction structures—see Casey and Panish [5].

[57] M. A. Haase, J. Qiu, J. M. DePuydt and H. Cheng, *Appl. Phys. Lett.* **59**, 1272 (1991).

[58] See Haase *et al.* [57] for the parameters of the first lasers. The most recent data is taken from the unpublished minutes of the workshop on *Wide-Band-Gap II-VI Materials for Lasers* sponsored by 3M in St. Paul, Minnesota, October 27-28, 1992. This data is similar to that given in C. T. Walker, J. M. DePuydt, M. A. Haase, J. Qiu and H. Cheng, presented at the 7th Trieste Semiconductor Symposium on Wide-Band-Gap Semiconductors, June 8-12, 1992, Trieste, to be published in *Physica B* (1993).

[59] Y. Lansari, J. Ren, B. Sneed, K. A. Bowers, J. W. Cook, Jr., and J. F. Schetzina, *Appl. Phys. Lett.* **61**, 2554 (1992).

[60] Y. Fan, J. Han, L. He, J. Saraie, R. L. Gunshor, M. Hagerott, H. Jeon, A. V. Nurmikko, G. C. Hua and N. Otsuka, *Appl. Phys. Lett.* **61**, 3160 (1992).

[61] H. Okuyama, K. Nakano, T. Miyajima and K. Akimoto, *J. Cryst. Growth* **117**, 139 (1992).

[62] H. Okuyama, T. Miyajima, Y. Morinaga, F. Hiei, M. Ozawa and K. Akimoto, *Electronics Letters* **28**, 1798 (1992).

Chapter 2

Heterojunctions for Light Emitters

2.1 Introduction

The schematic energy-band diagrams in Figure 2.1 show a simple *pn*-homojunction LED. This structure is the basis for most commercial LEDs, but requires that the same semiconductor be doped both *p*-type and *n*-type. Since most wide-bandgap materials can be doped either *p*-type or *n*-type but not both, it is natural to ask whether the *p* and *n* regions can be different materials, as shown in Figure 2.2.

MOCVD and MBE allow atomically abrupt changes in composition, and the resulting discontinuities in crystal properties are exploited in laser diodes and in a variety of electrical devices such as heterojunction bipolar transistors [1]. No commercial devices presently use heterojunctions to obtain *pn* heterojunctions where *pn* homojunctions are difficult to obtain. The idea is quite old, but there are few heterojunctions which meet the requirements on doping, band offsets and lattice match. The most successful system for heterojunction devices is $Al_xGa_{1-x}As$, which is nearly lattice-matched over the entire composition range, and which can produce band discontinuities and changes in index of refraction which are favorable

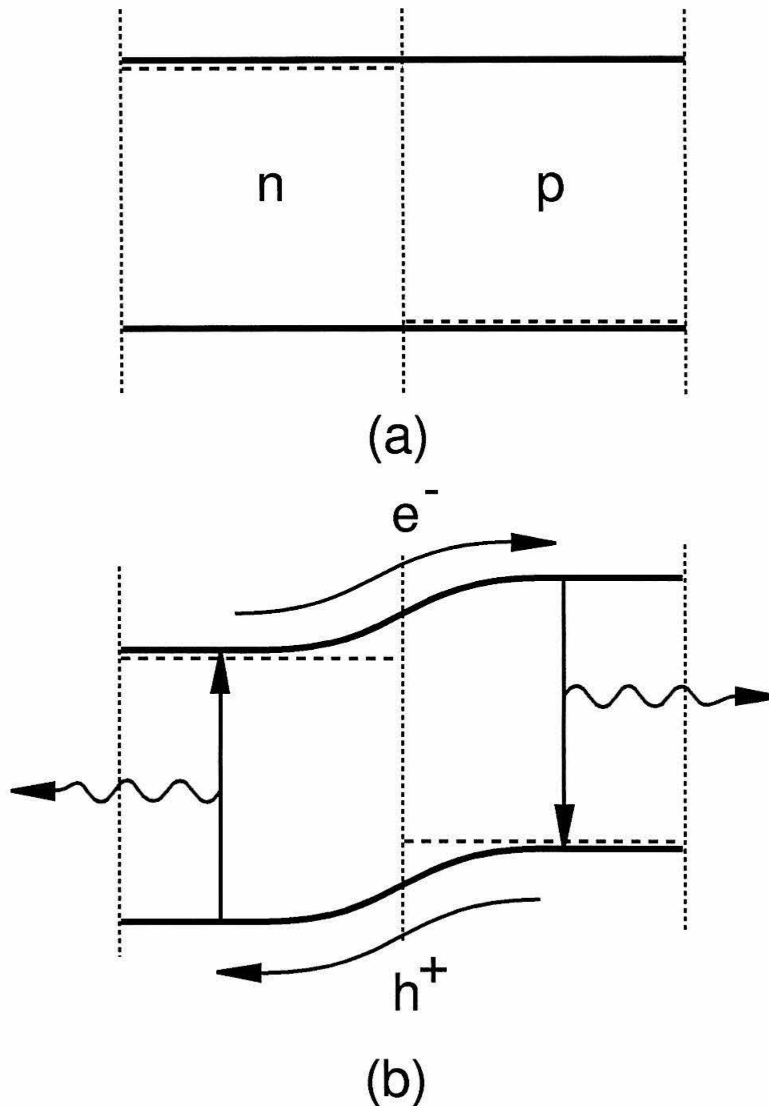

Figure 2.1: Schematic energy band diagrams for a simple homojunction LED. (a) Flatband. (b) Near operating bias. Electrons are injected from the n-type material into the p-type material where they recombine with holes, emitting photons with energy roughly equal to the bandgap of the semiconductor. Holes are injected from the p-type material into the n-type material, where they also recombine to emit photons.

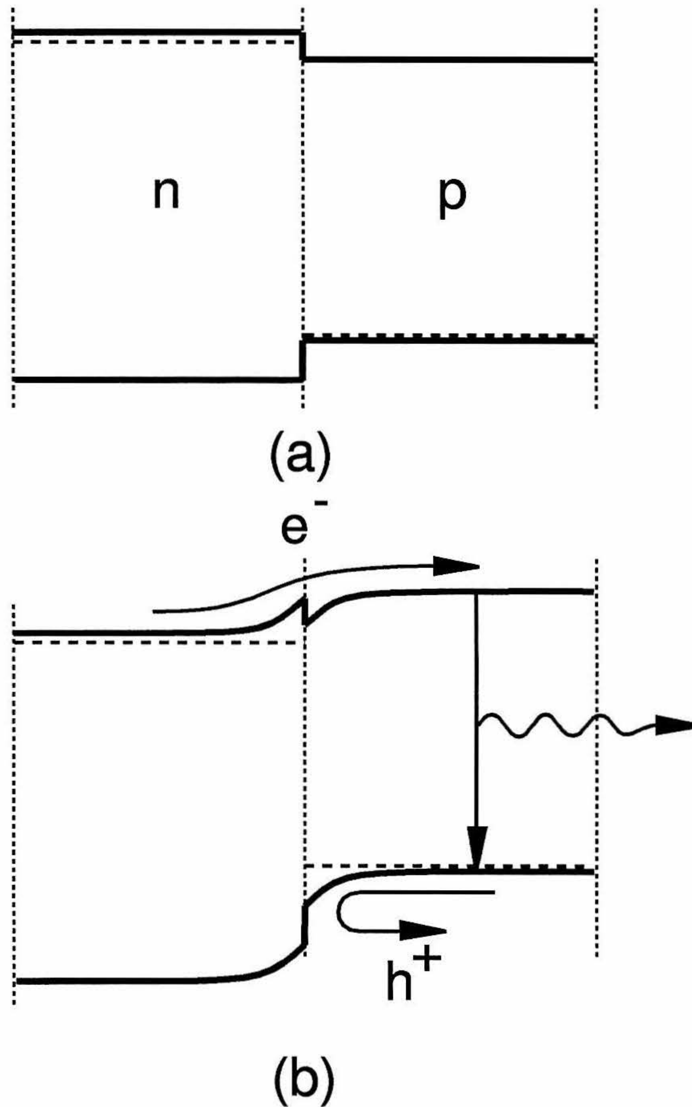

Figure 2.2: Schematic energy band diagrams for a heterojunction LED. (a) Flat-band. (b) Near operating bias. For the heterojunction shown, electrons are injected from the n-type material into the p-type material, while holes are blocked by the offset in the valence band. In general we require one non-blocking offset and close lattice match. It is often desirable to have one blocking offset.

for a variety of electrical and optical devices. For this system, heterojunctions are not necessary to avoid doping problems.

Figure 2.2 shows that in addition to lattice match, we require that at least one band offset allow carrier injection across the interface; this sketch is drawn with a conduction band offset that allows injection of electrons from the n-type material into the p-type material. The blocking offset in the valence band is desirable–if minority carriers were injected into both materials, light would be emitted at two wavelengths. In general, it is preferable to be able to control where carriers are injected and where they recombine.

Unfortunately the heterojunction in Figure 2.2 is a rarity; Figure 2.3 shows a more common situation. Since ZnSe can be doped n-type and has a blue bandgap, and since ZnTe can be doped p-type and has a green bandgap, the n-ZnSe/p-ZnTe heterojunction is an old favorite of II-VI researchers [2]. The 7% mismatch is disastrous for material quality, and the blocking offsets in both bands create accumulations of electrons and holes at the interface where they recombine nonradiatively through interface traps.

There are no obvious candidates for favorable heterojunctions among well-known wide-bandgap semiconductors. It might be possible to form heterojunctions with alloys or with some of the large number of lesser-known semiconductors, however searching for favorable heterojunctions is difficult since there are no general theories of band offsets which can accurately predict offsets for a wide variety of heterojunctions [5]. Even the few experimental values which are available often do not agree.

2.2 McCaldin diagrams

Figure 2.4 is an example of a diagram introduced by McCaldin [6] to help graphically display band offsets to aid in the search for useful heterojunctions. Instead of plotting bandgap versus lattice constant, as in Figure 1.1, we plot the band edges

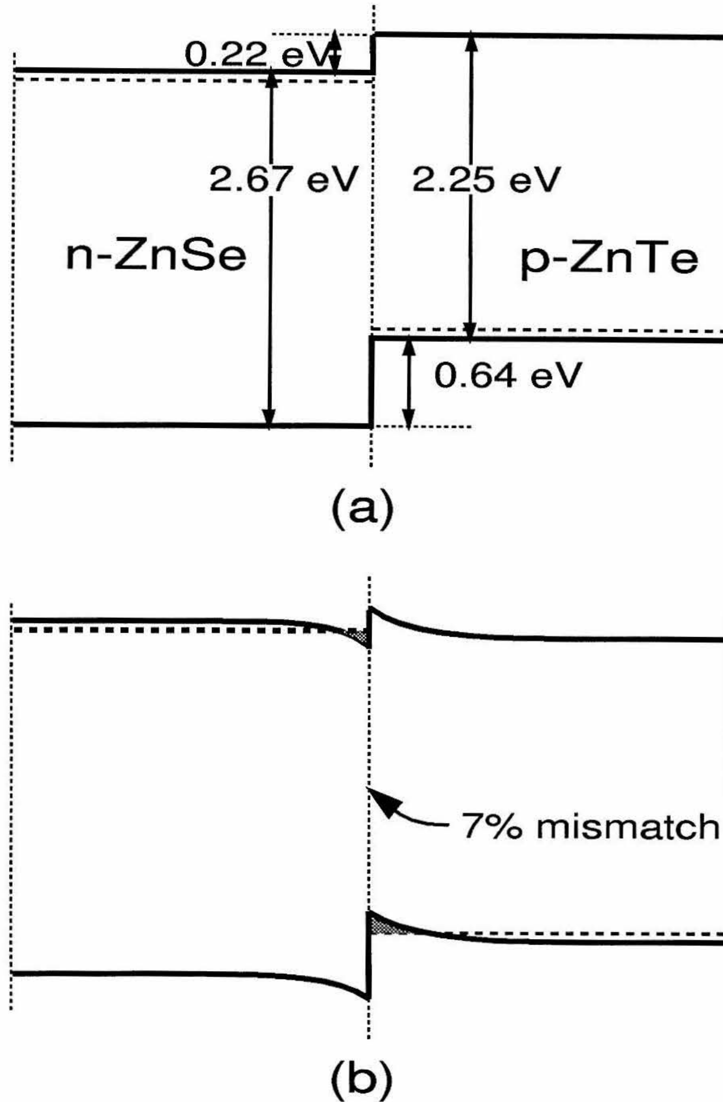

Figure 2.3: Example of an unfavorable heterojunction. (a) Flatband. The valence band offset was obtained from the measured CdSe/ZnTe offset [3, 4] by assuming the common-anion rule holds and neglecting the effect of strain. (b) Biased near operation. In *n*-ZnSe/*p*-ZnTe, both offsets are blocking and the lattice constants differ by about 7%. The blocking offsets cause accumulations of electrons and holes at the interface, driving strong nonradiative recombination through defect states at the interface. The 7% lattice mismatch creates a high density of misfit dislocations.

individually relative to the valence band of GaAs. This is an approximation, since band offsets often depend on details of growth, and are not necessarily transitive or even commutative, but these effects are generally small. The symbols for the band edges are filled if the material can be doped to that conductivity type, and are left open if they cannot. By plotting these diagrams for a large number of semiconductors according to a variety of models and experimental data, general trends become clear.

The four materials with low valence bands in Figure 2.4 (sulfides and selenides) are all difficult to dope p-type. When more materials are plotted, this trend becomes even more obvious. A similar trend is observed for materials with high conduction bands, which are difficult to dope n-type. Two materials in Figure 2.4 seem to violate this rule: the conduction band of ZnTe is plotted below that of AlSb, yet AlSb can be doped n-type while ZnTe cannot. McCaldin and McGill [8] suggested that this heterojunction could be used to inject electrons from n-AlSb into p-ZnTe.

When Yu *et al.* [9] measured the band offset in the AlSb/ZnTe system, they found that the theoretical model of Harrison [7]—which was used to plot the band edges in Figure 2.4—incorrectly predicts the sign of the conduction band offset between AlSb and ZnTe. The experimental values are shown in Figure 2.5. There are two important points here. First, band offsets must be experimentally measured for any systems identified as potentially useful. Second, AlSb and ZnTe do not violate the doping trend mentioned above: the conduction band of ZnTe lies above that of AlSb and is more difficult to dope n-type. This doping trend is contrary to our desire for favorable offsets. We need n-dopable materials with high conduction bands or p-dopable materials with low valence bands so that at least one offset will not be blocking. There seems to be a trend in nature opposing the heterojunction configuration we need for large-bandgap semiconductors. Of course, large-bandgap homojunctions are also difficult, because at least one band

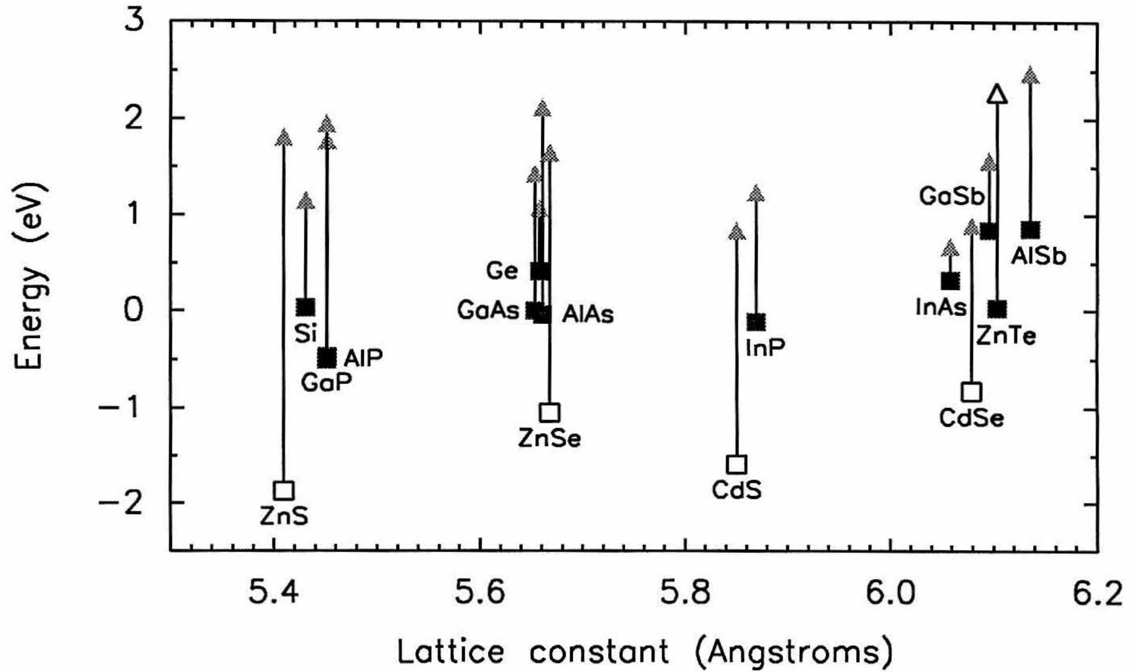

Figure 2.4: McCaldin diagram [6]: a plot of band edges versus lattice constant for some common semiconductors. The conduction-band edge is marked with a filled triangle if the material can be doped n-type, and with an open triangle if it cannot. The valence-band edge is marked with a filled square if the material can be doped p-type, and an open square if it cannot. Band offsets can be read directly from the diagram. The band positions in this diagram are plotted according to the theory of Harrison [7]. The energy zero is chosen to be the valence band of GaAs. Lattice constants of wurtzite materials are converted to equivalent Zn-blende cubic lattice parameters assuming the volume of the unit cell remains constant.

edge in a large-bandgap material must lie very high or very low.[1]

We could could consider ever more obscure semiconductors in hopes of finding a lattice-matched junction with favorable offsets, or a wide bandgap *pn* homojunction, but the doping trends evident in the McCaldin diagrams suggest that we are unlikely to find what we want. We propose to take what nature will give us—dopability and lattice match—and design a structure which works around a blocking offset.

2.3 *n*-CdSe/*p*-ZnTe

Figure 2.6(a) shows a flatband diagram for *n*-CdSe/*p*-ZnTe which is the only closely-lattice-matched *pn* heterojunction between II-VI binary compounds. The equilibrium crystal structure of CdSe is wurtzite, but its preference for this structure is not strong and thick layers of CdSe can be grown in Zn-blende form on (100) Zn-blende substrates [10]. The lattice constant of cubic CdSe is 6.077 Å [10], while that of ZnTe is 6.104 Å. Several hundred Å of cubic CdSe can be grown on ZnTe without exceeding the equilibrium critical thickness.

ZnTe tends to be *p*-type if grown Te-rich, while CdSe tends to be *n*-type and can be doped to free electron concentrations well in excess of $\times 10^{19}$ /cm^3. The blocking offset in the valence band prevents hole injection into the CdSe which would result in emission of red light. Unfortunately the blocking offset in the conduction band is even larger. Under forward bias, large accumulations of electrons and holes form at the interface, causing strong nonradiative recombination and little or no light emission [3].

[1] At shorter lattice constants the "region of dopability" on McCaldin diagrams seems to open up. For example, SiC can be doped both *p*- and *n*-type in spite of having a large bandgap. The recent progress on *p*-type doping of GaN may also be an example of this. The disadvantages of materials with shorter lattice constants include fewer choices for lattice-matched substrates and for heterojunctions, which are necessary for carrier and light confinement in laser diodes.

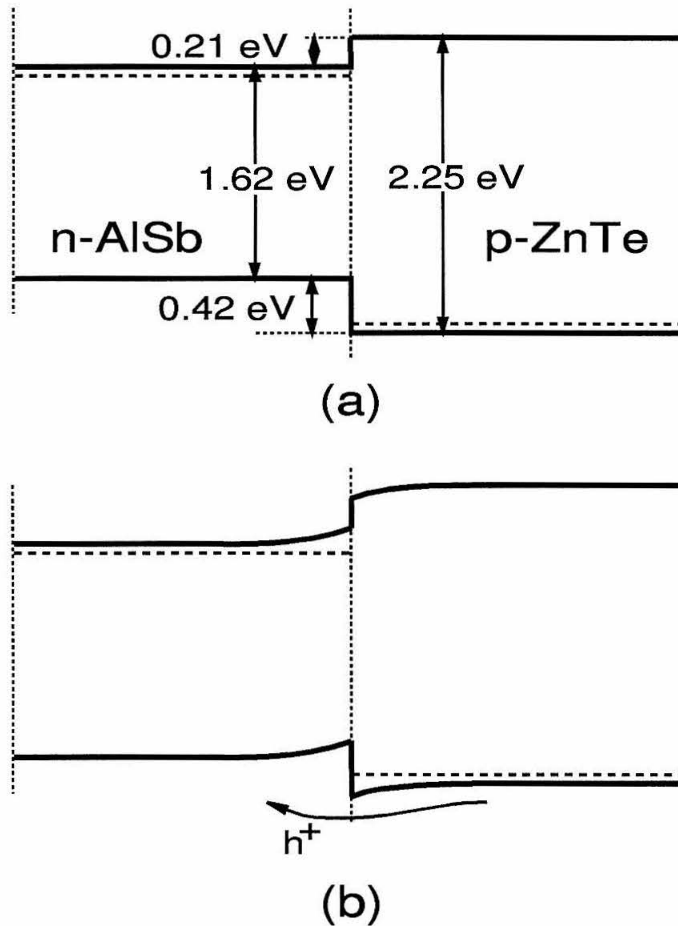

Figure 2.5: The n-AlSb/p-ZnTe heterojunction, identified by McCaldin and McGill [8] as a possible basis for light-emitting structures. The valence-band offset does not block the undesirable injection of holes from the ZnTe into the AlSb. If the conduction band offset were not blocking, or if it was blocking but sufficiently small, then by doping the AlSb heavily n-type while leaving the ZnTe lightly p-type, the hole current could be suppressed sufficiently to make a reasonably efficient light emitter. Subsequent accurate measurements of the valence-band offset by Yu *et al.* [9] gave the band offsets shown in the figure; the conduction band offset is blocking, but small enough to make an LED marginally feasible.

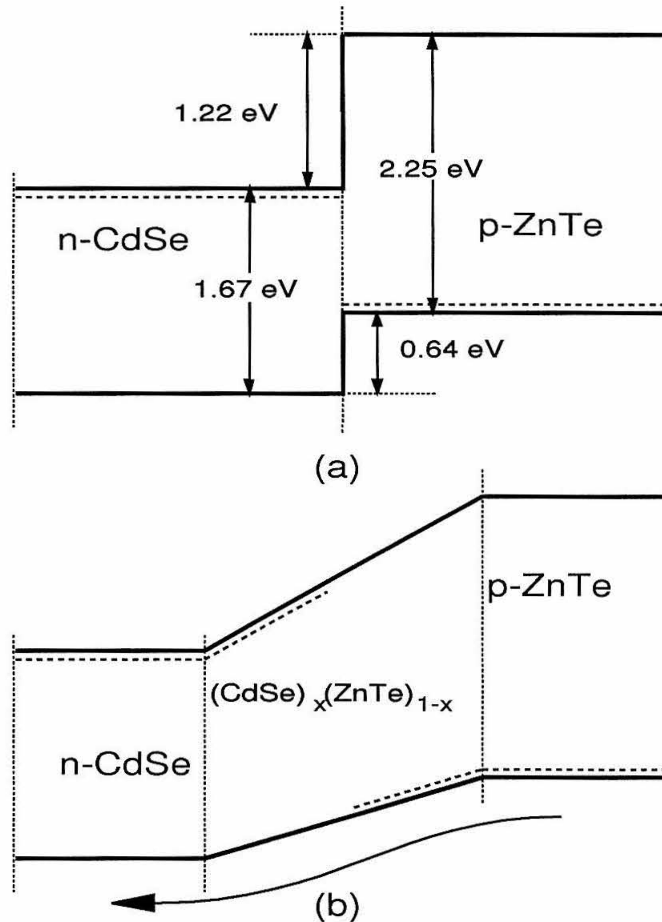

Figure 2.6: n-CdSe/p-ZnTe: the only closely-lattice-matched pn heterojunction between binary II-VI compounds. (a) Flatband diagram of the abrupt junction. The valence-band offset blocks the undesirable injection of holes from the ZnTe into the CdSe. The conduction-band offset is extremely unfavorable for the injection of electrons into the ZnTe. (b) Flatband diagram of a simple graded junction. Grading with the $(CdSe)_x(ZnTe)_{1-x}$ pseudobinary maintains lattice match and avoids large accumulation regions, but the barrier to electron injection into the ZnTe is much larger than the barrier to hole injection into the CdSe, hence the device would emit predominantly red light [3, 4].

Figure 2.6(b) shows an attempt to remove the blocking offset in the conduction band by grading through the lattice-matched pseudobinary $(CdSe)_x(ZnTe)_{1-x}$. Ignoring the difficulties in controlling the alloy concentration of this quaternary to maintain lattice match, and ignoring the large miscibility gaps which occur in this quaternary at low temperatures [11], this structure is still an inefficient green-light emitter. Since the offset in the valence band is much less than that in the conduction band, most of the current will be hole injection into the CdSe.

We need to grade the offset in the conduction band while leaving an abrupt offset in the valence band. Since the position of the valence band in these materials is determined mainly by the anion, the abrupt offset in the valence band comes from the abrupt change from selenide to telluride. Thus we need to grade the conduction band by changing the cation, and put a blocking offset in the valence band with an abrupt change in the anion. To grade the conduction band of the CdSe up to that of ZnTe, we need a cation which will open up the bandgap of CdSe much faster than Zn. For this we will have to look outside of column IIb in the periodic table.

2.4 New material systems

Figure 2.7 shows another McCaldin diagram, this time including II-VI chalcogenides with transition metal cations or column IIa cations. These compounds are much less well known than II-VI chalcogenides with column IIb cations. Many of these materials have very large bandgaps and can be alloyed with the more common chalcogenides to open their bandgaps. There are no lattice-matched ternaries analogous to $Al_xGa_{1-x}As$, but there are cations which will decrease or increase the lattice constants of the Zn and Cd chalcogenides: Be is smaller than Zn; Mg and Mn are intermediate between Zn and Cd; and Ca and Sr are larger than Cd [22]. Okuyama *et al.* [15] have recently reported the use of Mg to form a wide-bandgap cladding material for blue lasers lattice-matched to GaAs. By alloying ZnSe with S

(smaller than Se) and Mg (larger than Zn) they open the bandgap and decrease the index of refraction while maintaining lattice match to GaAs, which has a lattice constant slightly smaller than ZnSe.

In Chapter 3 we will discuss the use of Mg alloys to overcome the blocking conduction band offset in the n-CdSe/p-ZnTe heterojunction. Finally in Chapter 4 we describe the details of MBE growth of this new material system.

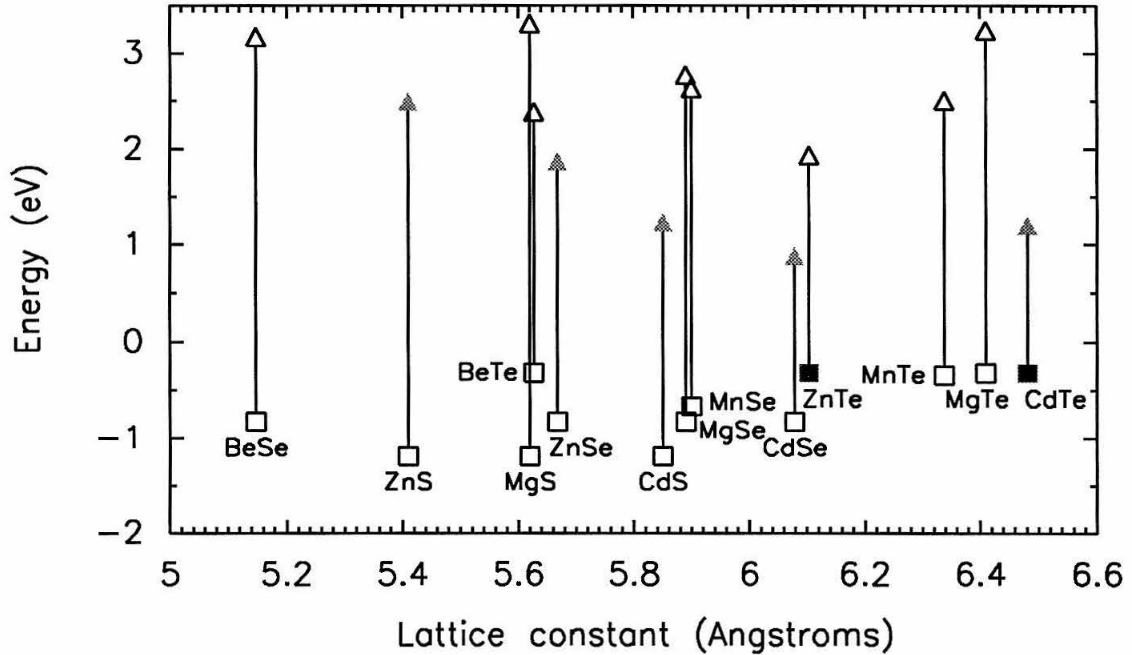

Figure 2.7: McCaldin diagram including some of the Be, Mg and Mn chalcogenides. Alloys of these compounds with the Zn and Cd chalcogenides offer the possibility of a "bandgap engineering" solution to the problem of making II-VI light emitters. All of the Be, Mg and Mn compounds are plotted as undopable, though BeTe (and probably the other tellurides) is p-dopable. Offsets for the Zn and Cd chalcogenides are plotted according to the common-anion rule of McCaldin *et al.* [12]. The Be and Mg chalcogenides are also plotted assuming they obey the common anion rule. The MnTe offset is plotted according to the experimental value from Change *et al.* [13]; MnSe according to Asonen *et al.* [14]. Bandgap and lattice constant of MgSe and MgS are from Okuyama *et al.* [15]; MgTe bandgap from Marine *et al.* [16]; lattice constants of MgTe and the Be compounds from Villars *et al.* [17]; bandgaps of Be compounds from Yim *et al.* [18]; bandgap of MnTe from Furdyna [19]; bandgap of MnSe from Asonen *et al.* [14]; lattice constant of MnTe from Pessa and Jylhä [20]; lattice constant of MnSe from Kolodziejski *et al.* [21].

Bibliography

[1] For a review of semiconductor heterojunctions, including a variety of applications, see A. G. Milnes, *Solid–State Electron.* **29**, 99 (1986).

[2] See, for example, S. Fujita, S. Arai, F. Itoh and T. Sakaguchi, *J. Appl. Phys.* **46**, 3070 (1975); or P. A. Gashin, L. F. Komolova, G. V. Saparin, A. V. Simashkevich and D. A. Sherban, *Izvestiya Akademii Nauk SSSR* **40**, 2005 (1976); or F. Firszt and H. J. Łożykowski, *Acta Physica Polonica* **A64**, 9 (1983).

[3] M. C. Phillips, E. T. Yu, Y. Rajakarunanayake, J. O. McCaldin, D. A. Collins and T. C. McGill, *J. Cryst. Growth* **111**, 820 (1991).

[4] E. T. Yu, M. C. Phillips, J. O. McCaldin and T. C. McGill, *J. Vac. Sci. Technol. B* **9**, 2233 (1991).

[5] For a detailed review of band offset theories and experiments, see E. T. Yu, J. O. McCaldin and T. C. McGill, *Solid State Phys.* **46**, 1 (1992).

[6] J. O. McCaldin, *J. Vac. Sci. Technol. A* **8**, 1188 (1990).

[7] W. A. Harrison, *J. Vac. Sci. Technol.* **14**, 1016 (1977).

[8] J. O. McCaldin and T. C. McGill, *J. Vac. Sci. Technol. B* **6**, 1360 (1988).

[9] E. T. Yu, E. T. Croke, D. H. Chow, D. A. Collins, M. C. Phillips, T. C. McGill, J. O. McCaldin and R. H. Miles, *J. Vac. Sci. Technol. B* **8**, 908 (1990).

[10] N. Samarth, H. Luo, J. K. Furdyna, S. B. Qadri, Y. R. Lee, A. K. Ramdas and N. Otsuka, *Appl. Phys. Lett.* **54**, 2680 (1989).

[11] V. Leute, *Solid State Ionics* **17**, 185 (1985).

[12] J. O. McCaldin, T. C. McGill and C. A. Mead, *Phys. Rev. Lett.* **36**, 56 (1976).

[13] S.-K. Chang, A. V. Nurmikko, J.-W. Wu, L. A. Kolodziejski and R. L. Gunshor, *Phys. Rev. B* **37**, 1191 (1988).

[14] H. Asonen, J. Lilja, A. Vuoristo, M. Ishiko and M. Pessa, *Appl. Phys. Lett.* **50**, 733 (1987).

[15] H. Okuyama, K. Nakano, T. Miyajima and K. Akimoto, *Jpn. J. Appl. Phys.* **30**, L1620 (1991).

[16] J. Marine, T. T. D'Ouville, B. Schaub, A. Laugier, D. Barbier, J. C. Guillaume, J. F. Rommeluere and J. Chevallier, *J. Elec. Mater.* **7**, 17 (1978).

[17] P. Villars and L. D. Calvert, *Pearson's Handbook of Crystallographic Data for Intermetallic Phases* (American Society for Metals, Metals Park, Ohio, 1985).

[18] W. M. Yim, J. P. Dismukes, E. J. Stofko and R. J. Paff, *J. Phys. Chem. Solids* **33**, 501 (1972).

[19] J. K. Furdyna, *J. Vac. Sci. Technol. A* **4**, 2002 (1986).

[20] M. Pessa and O. Jylhä, *Appl. Phys. Lett.* **45**, 646 (1984).

[21] L. A. Kolodziejski, R. L. Gunshor, N. Otsuka, S. Datta, W. M. Becker and A. V. Nurmikko, *IEEE J. Quantum Electron.* **22**, 1666 (1986).

[22] For Ca and Sr sulfides, see T. Kobayashi, K. Susa and S. Taniguchi, *J. Solid State Chem.* **33**, 203 (1980).

Chapter 3

The Graded Injector

3.1 Proposal for a new light-emitting structure

Figure 3.1 shows the calculated band profile for an abrupt *n*-CdSe/*p*-ZnTe heterojunction. This figure and Figure 3.2, which shows the calculated carrier densities for the same junction, verify the assertions made in Chapter 2 regarding this heterojunction. At 1.25 V bias, practically no carriers are injected across the heterojunction, yet large accumulations of electrons and holes have formed at the interface where they will recombine nonradiatively.

In Section 2.3 we proposed to grade the conduction band of the CdSe up to that of the ZnTe while leaving an abrupt offset in the valence band. Ideally we would like to substitute another cation for Cd to open up the bandgap without changing the lattice constant, but there is no cation which will accomplish this. Figure 3.3 is a McCaldin diagram including the $Mg_xCd_{1-x}Se$ alloy system. Substituting Mg for Cd opens up the bandgap quickly, but also decreases the lattice constant. This places an upper limit on the thickness of the graded region which can be grown without exceeding the critical thickness for generation of misfit dislocations.

The band offsets for the CdSe/ZnTe heterojunction were shown in Figure 2.6(a). To grade the conduction band of the CdSe up to that of ZnTe we need to increase

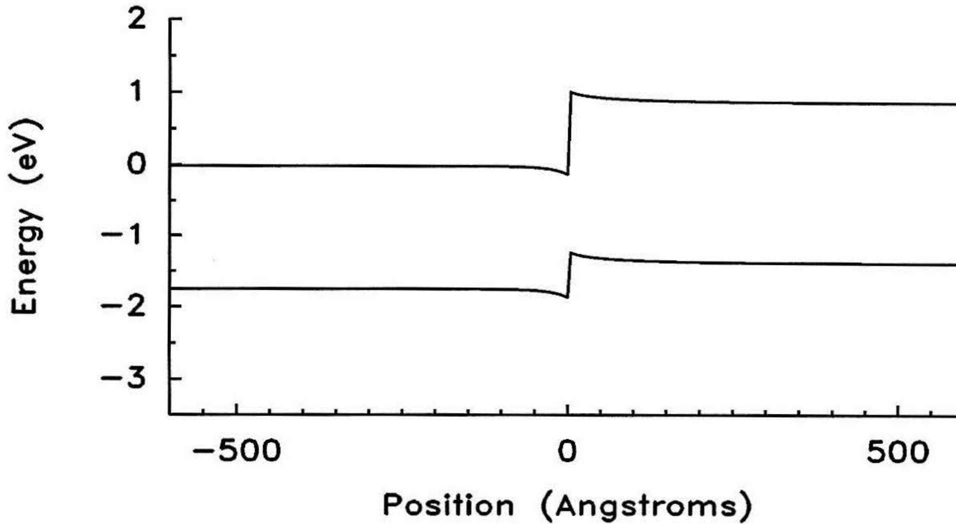

Figure 3.1: Calculated band profile for an abrupt n-CdSe/p-ZnTe heterojunction at 1.25 V forward bias, from a detailed computer model by Wang *et al.* [1]. At this bias there is still a large barrier to injection of electrons into the ZnTe, yet accumulations of electrons and holes are forming at the heterointerface (see Figure 3.2).

the bandgap of the CdSe by 1.22 eV to 2.89 eV. Since the bandgap of pure Zn-blende MgSe is extrapolated to be 3.6 eV [3], the $Mg_xCd_{1-x}Se$ alloy at the peak of the grading must have $x = 0.63$. This alloy is lattice-mismatched to the ZnTe substrate by 2.4%, which is a fairly large lattice mismatch, but this is only at the peak of the grading. Predicting the maximum thickness to which a strained epilayer can be grown without generating misfit dislocations is quite difficult; various theories exist, but none are accurate for a wide range of material systems and growth parameters. We concluded that the layer must be less than 200–300 Å to remain coherent.

As we decrease the thickness of the grading, at some point the device will behave like an abrupt junction. We need to know whether the maximum thickness allowed by lattice-mismatch considerations is adequate to fix the problems of the abrupt junction. A detailed computer model of graded-$Mg_xCd_{1-x}Se$ devices indicates *that*

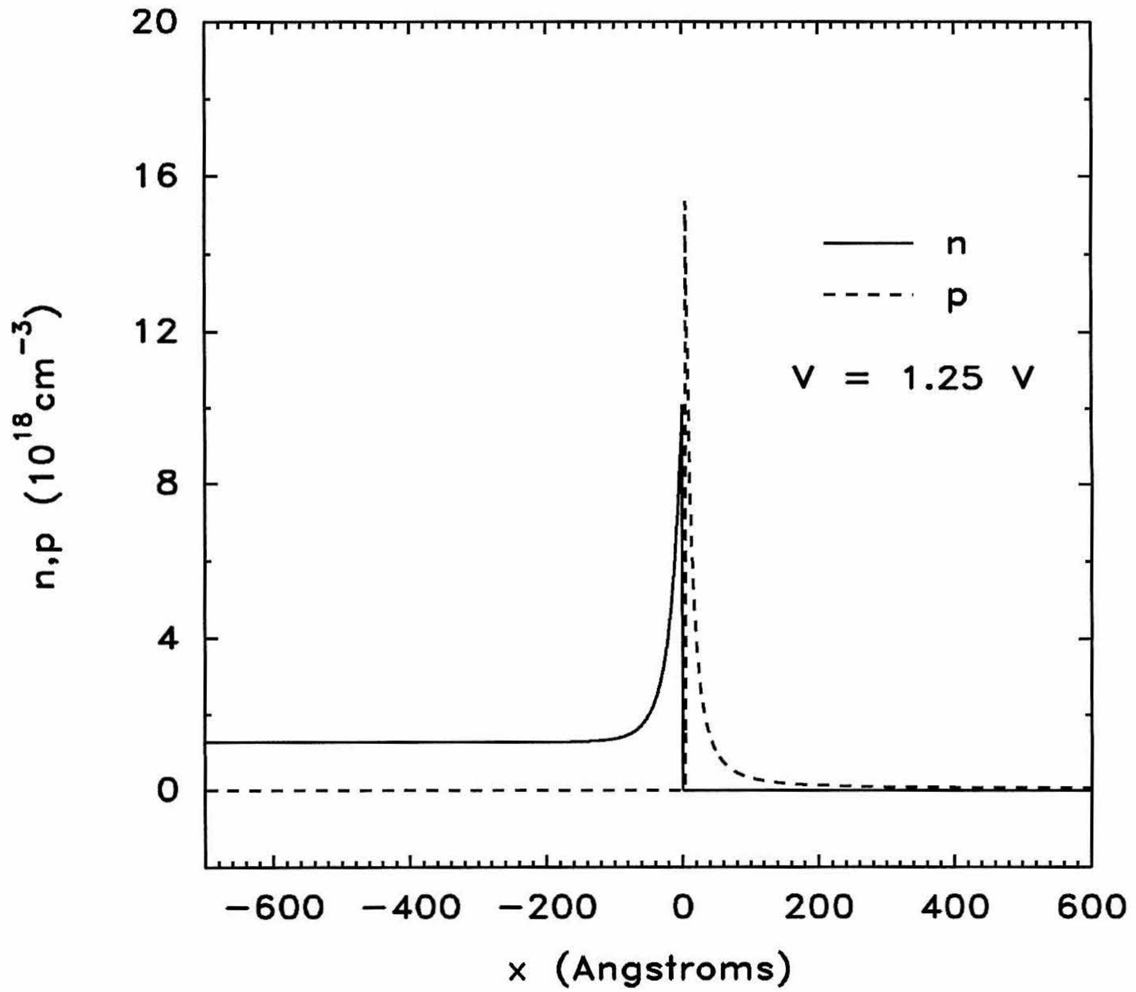

Figure 3.2: Calculated carrier densities for the abrupt n-CdSe/p-ZnTe heterojunction shown in Figure 3.1.

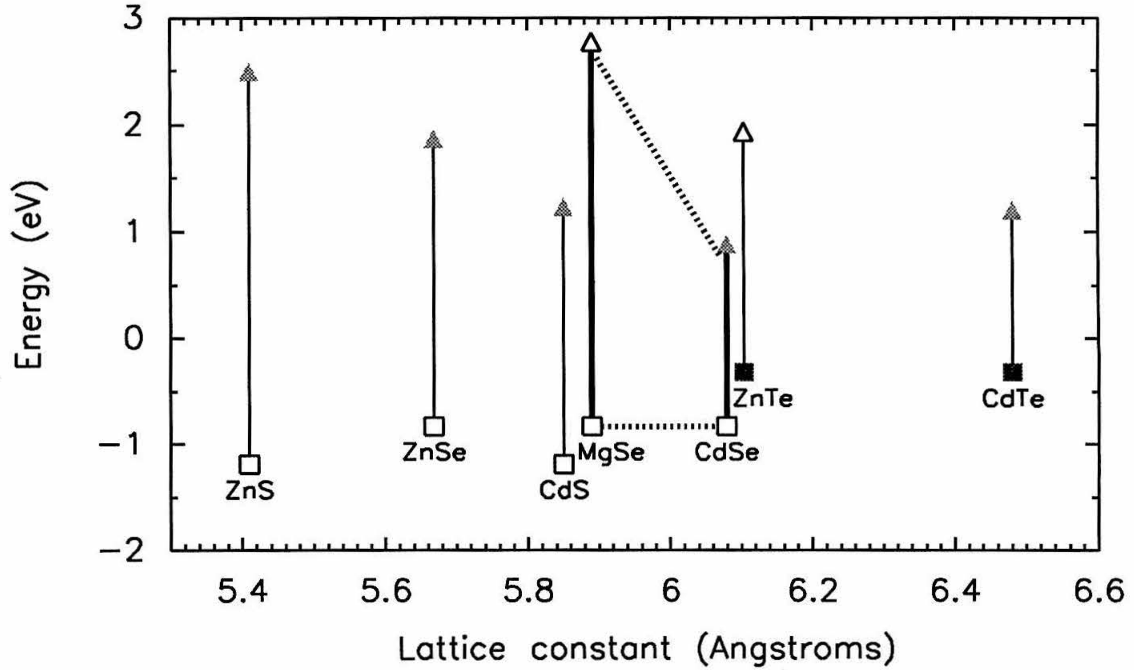

Figure 3.3: McCaldin diagram including the $Mg_xCd_{1-x}Se$ alloy system. Offsets for the Zn and Cd chalcogenides are plotted according to McCaldin *et al.* [2]; MgSe is assumed to obey the common-anion rule. Bandgap and lattice constant are for the Zn-blende form which can be grown by MBE on (100) Zn-blende substrates [3].

a 300 Å graded region does not behave like an abrupt junction [1]. Figure 3.4 shows a flatband diagram of the proposed device, and the calculated band profile at 2.0 V forward bias. Figure 3.5 gives the calculated carrier densities at the same bias. At this bias there is substantial electron injection into the ZnTe, yet the accumulation regions are quite small and are spatially separated by the width of the grading so that they will not cause nonradiative recombination.

This grading scheme does not rely on doping in the graded region to keep the conduction band close to the Fermi level. If this were the case, the grading would need to be long compared to the depletion length, and since the $Mg_xCd_{1-x}Se$ alloys are probably not heavily n-dopable at high Mg concentrations, the grading would have to be much thicker than 200–300 Å. Doping in the graded region is desirable because it will help prevent charging of any traps present in the $Mg_xCd_{1-x}Se$, but doping in the graded region is not fundamentally important for graded injection.

Figure 3.4 introduces the simplest form of graded-injection device. Electrons are injected into bulk ZnTe, where some of them will recombine radiatively to emit green light. More complicated heterostructures, such as the blue LED shown in Figure 3.6, are also possible. Laser structures will require carrier-confining regions such as quantum wells, and light-confining wave guides, probably formed with $Mg_xZn_{1-x}Te$ alloys or eventually with lattice-matched quaternaries.

Finally, note that the use of graded injection is not necessarily limited to the material system shown in Figure 3.4. The idea is to use smooth grading in one band while introducing an abrupt offset in the other band to obtain efficient minority carrier injection in spite of an unfavorable band alignment. Since, as was pointed out in Section 2.2, the band alignments between large-bandgap p-dopable and n-dopable semiconductors are generally unfavorable for minority carrier injection, graded injection may be important in other wide-bandgap systems.

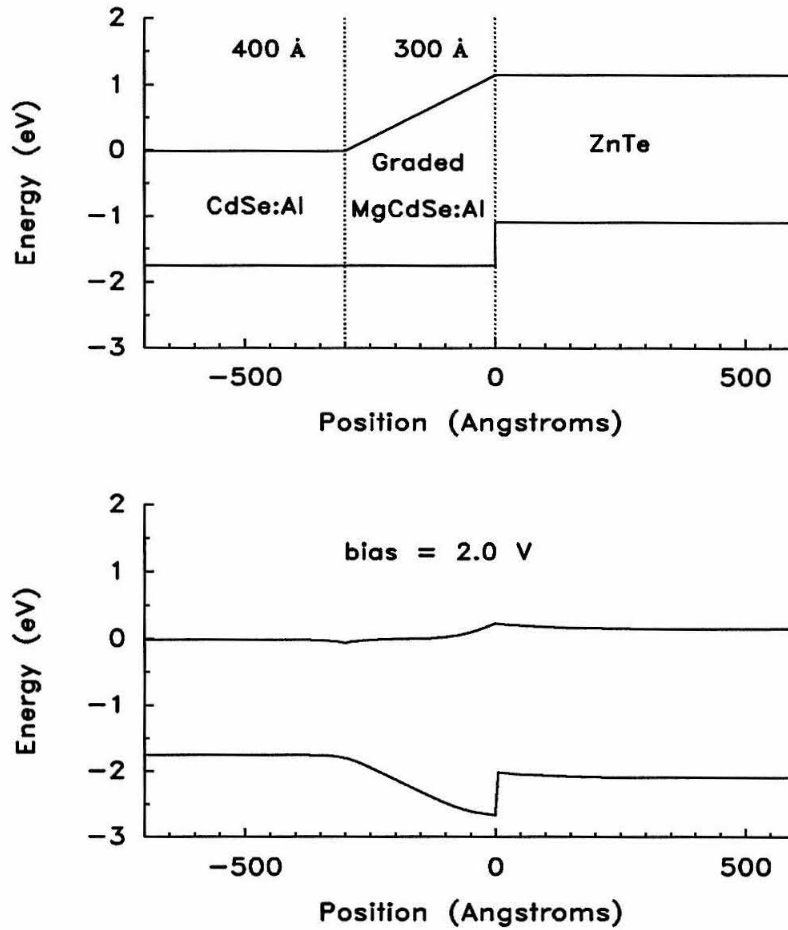

Figure 3.4: Band diagrams for a graded-$Mg_xCd_{1-x}Se$ light emitter [4]. Top: flat-band. Bottom: calculated band profile at 2.0 V forward bias [1]. At this bias there is substantial injection of electrons from the CdSe into the ZnTe. Hole injection into the CdSe is blocked by the large valence-band offset.

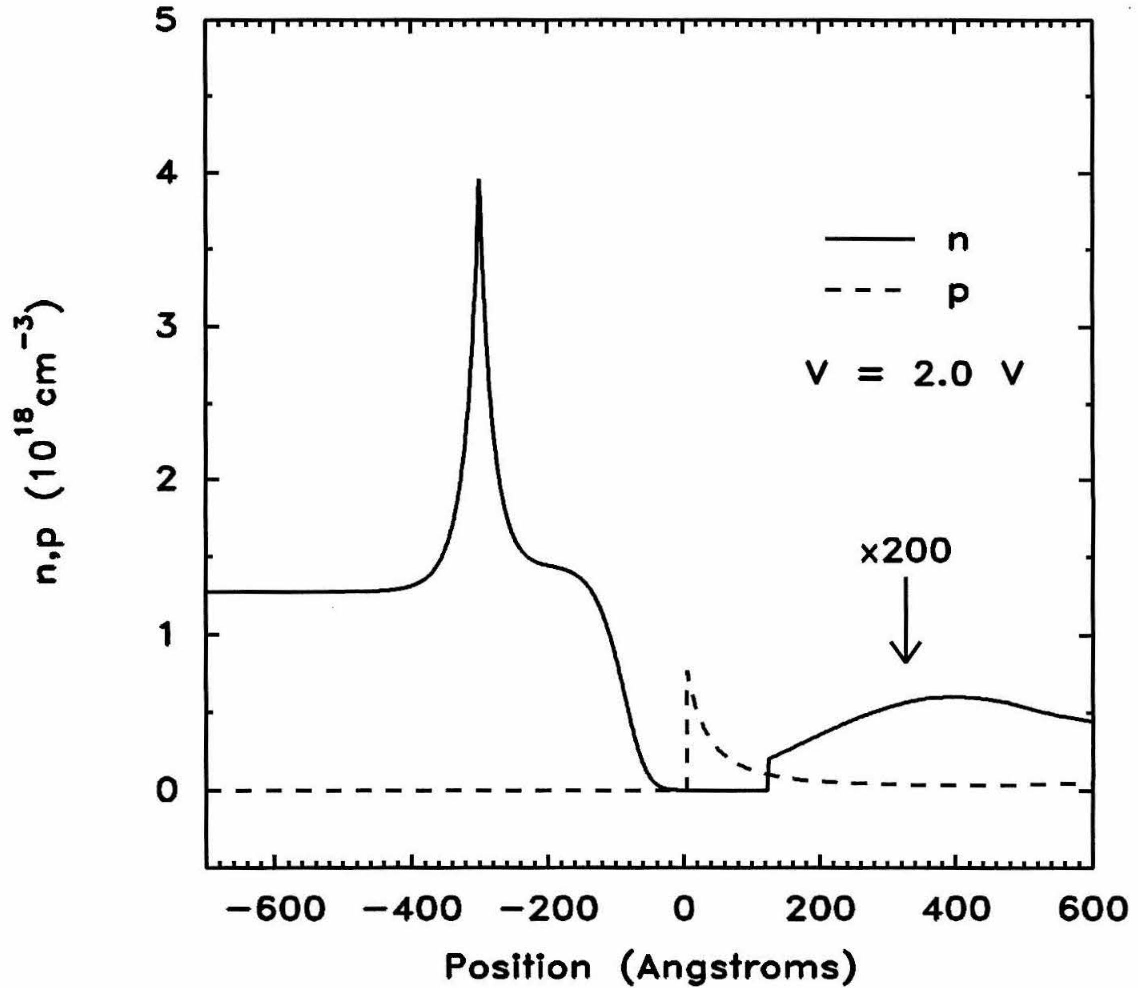

Figure 3.5: Calculated carrier densities in a graded-$Mg_xCd_{1-x}Se$ device at 2.0 V forward bias. The accumulation regions are small and spatially separated by the width of the graded region. Note the electrons injected into the ZnTe.

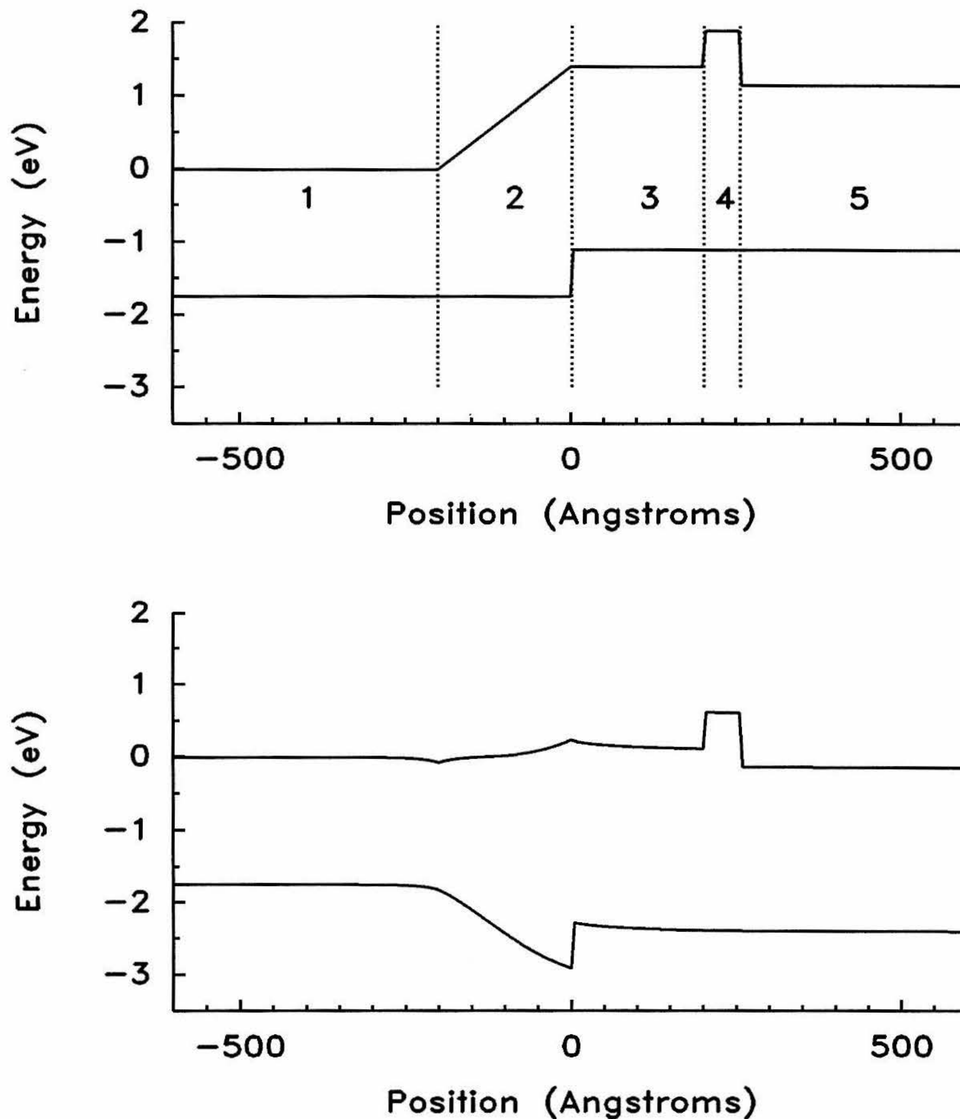

Figure 3.6: Graded-$Mg_xCd_{1-x}Se$ blue LED. Top: flatband. Bottom: calculated band profile at 2.25 V. The grading is extended to a higher Mg concentration, and the bandgap of the ZnTe is increased by alloying with MgTe. A narrow region of higher Mg concentration is included to prevent the injected electrons from diffusing beyond the $Mg_xZn_{1-x}Te$ recombination region. Numbered regions are (1) n-CdSe:Al, (2) graded-$Mg_xCd_{1-x}Se$, (3) $Mg_xZn_{1-x}Te$ recombination region, (4) $Mg_xZn_{1-x}Te$ electron-confinement region, (5) p-type ZnTe.

3.2 Experiment

In Section 3 we proposed a new injection scheme for use in wide-bandgap light emitters, and suggested a material system for fabricating devices based on this proposal. Turning these ideas into devices is a formidable challenge. MBE of II-VI materials is still much less common, and hence less well developed, than III-V MBE. Most II-VI MBE is done with ZnSe-based systems, so the growth of ZnTe-based systems is even less well developed. Standard procedures for preparing, mounting, and deoxidizing substrates before growth, and for metallization, photolithography, ohmic contacting, and wire bonding do not exist for wide-bandgap II-VI materials, and procedures for III-Vs are often unsuitable for II-VIs.

This research and the report by Okuyama *et al.* [3] represent the first growths of Mg chalcogenides by MBE. The most critical region of the device, a graded region less than 300 Å thick, is formed with these relatively unknown compounds. Semiconductor-grade Mg is not commercially available, and apparently no one is presently capable of the special distillation process required to exceed 99.99% purity; we spent more than a year tracing down the remnants of a supply of Mg purified over 20 years ago.

Fabricating a working light emitter to demonstrate the validity our ideas requires some level of control over all the steps from growth through device fabrication. Most of the problems have been resolved adequately for demonstration LEDs, and some of the solutions will be discussed in Chapter 4. In the remainder of this chapter we will describe the green LEDs which we fabricated to demonstrate graded injection, and then address the major remaining obstacle to fabrication of high-efficiency devices: *p*-type doping of ZnTe during MBE growth.

3.2.1 Graded-$Mg_xCd_{1-x}Se$ green LED

The schematic flatband diagram in Figure 3.7 is an example of the green LED structures we grew to test the graded-injection approach. We calibrated the peak

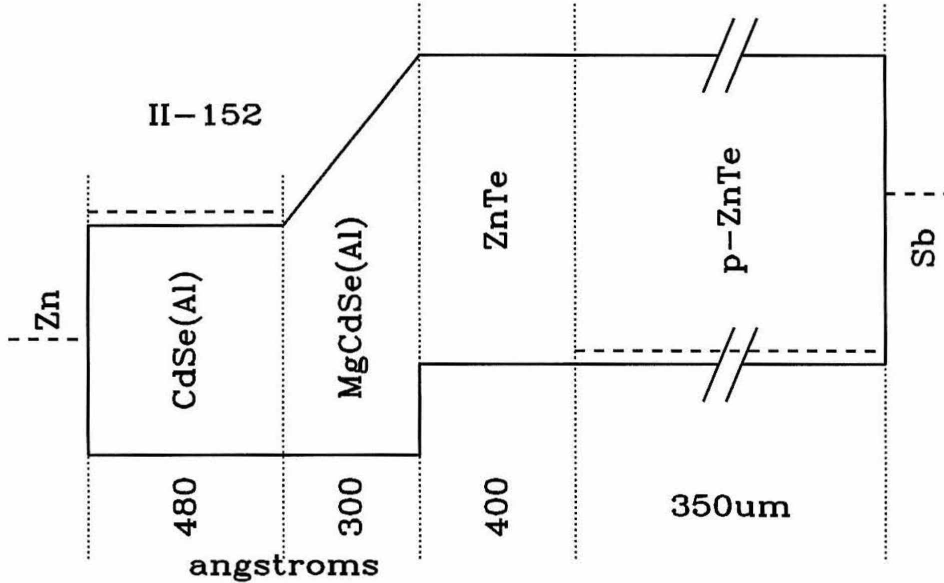

Figure 3.7: Schematic flatband diagram of a simple graded-$Mg_xCd_{1-x}Se$ green LED structure, sample II-152. The peak magnesium concentration of the $Mg_xCd_{1-x}Se$ region is approximately $x = 0.62$. Substrate is (100)-oriented, single-crystal, p-type ZnTe with resistivity $\rho = 1.3\ \Omega$ cm and hole concentration $p = 4.6\ \times 10^{16}$ /cm^3. The Zn cap was applied in the growth chamber; additional Zn and the Sb back contact were applied after removing the sample from vacuum.

concentration of the Mg by XPS on bulk layers of $Mg_xCd_{1-x}Se$, and checked the accuracy of the XPS measurements with electron microprobe analysis. There are some uncertainties in the dependence of the bandgap of $Mg_xCd_{1-x}Se$ on x, and if the grading does not bring the conduction band of the $Mg_xCd_{1-x}Se$ up to that of the ZnTe, a blocking offset will remain in the conduction band. On the other hand, the computer device modeling shows that extending the grading slightly too high does not affect device performance, therefore we chose the peak concentration so that we were more likely to overshoot than undershoot the grading.

To obtain the grading we simply shut off the power to the Mg effusion cell when the Mg, Cd and Se shutters opened. To control the thickness of the grading, we

had previously measured the decrease in the Mg flux after shutting off the effusion cell power using an ion-tube flux monitor and a residual gas analyzer. We then adjusted the CdSe growth rate so that the grading would occur over 200–300Å. The device modeling shows that the exact shape of the grading is not important.

After removing the samples from UHV, we evaporated additional Zn on the epilayer and an Sb contact on the back, then cleaved the sample into $\approx$ 1 mm $\times$ 1 mm chips. We isolated mesa diodes 110 μm in diameter by photolithography and wet etching. A sketch of the resulting device structure is shown in Figure 3.8. This structure is satisfactory for measuring electrical characteristics, but terrible for emitting light. The Zn cap and Sb back contact absorb most of the light which strikes them. The critical angle for ZnTe is less than 19°, so only light striking the edges of the dice at near-normal incidence can escape. Most of the light which does escape comes from a narrow region around the edge of the mesa where the Zn cap etches back under the photoresist, exposing the CdSe.

Figures 3.9 and 3.10 are linear and log plots of the room-temperature *J-V* characteristics of the green LED described in Figures 3.7 and 3.8. Figure 3.11 shows a comparison of the forward bias electrical characteristics of this device with the ZnSe:N blue-green laser of Haase *et al.* [5] and the ZnSe:N LED with an inverted structure reported by Jeon *et al.* [6]. At less than 10 V the current densities in the graded device are hundreds of A/cm^2, roughly the current densities required for good laser diodes. This data was taken at room temperature without pulsing and without special heat sinking. While these *J-V* characteristics compare quite favorably with the ZnSe:N devices, the operating voltage is still much higher than predicted by our simulations, which show that the device should turn on like an ordinary diode and operate at voltages near the bandgap of ZnTe. The high operating voltage is due to several shortcomings of this primitive stage of our device. Oriented, single crystal ZnTe substrates are not yet a standard commercial item, and the best substrates we have obtained have poor structural quality and resistivities of about 1.3 Ω cm. This produces the large series resistance evident

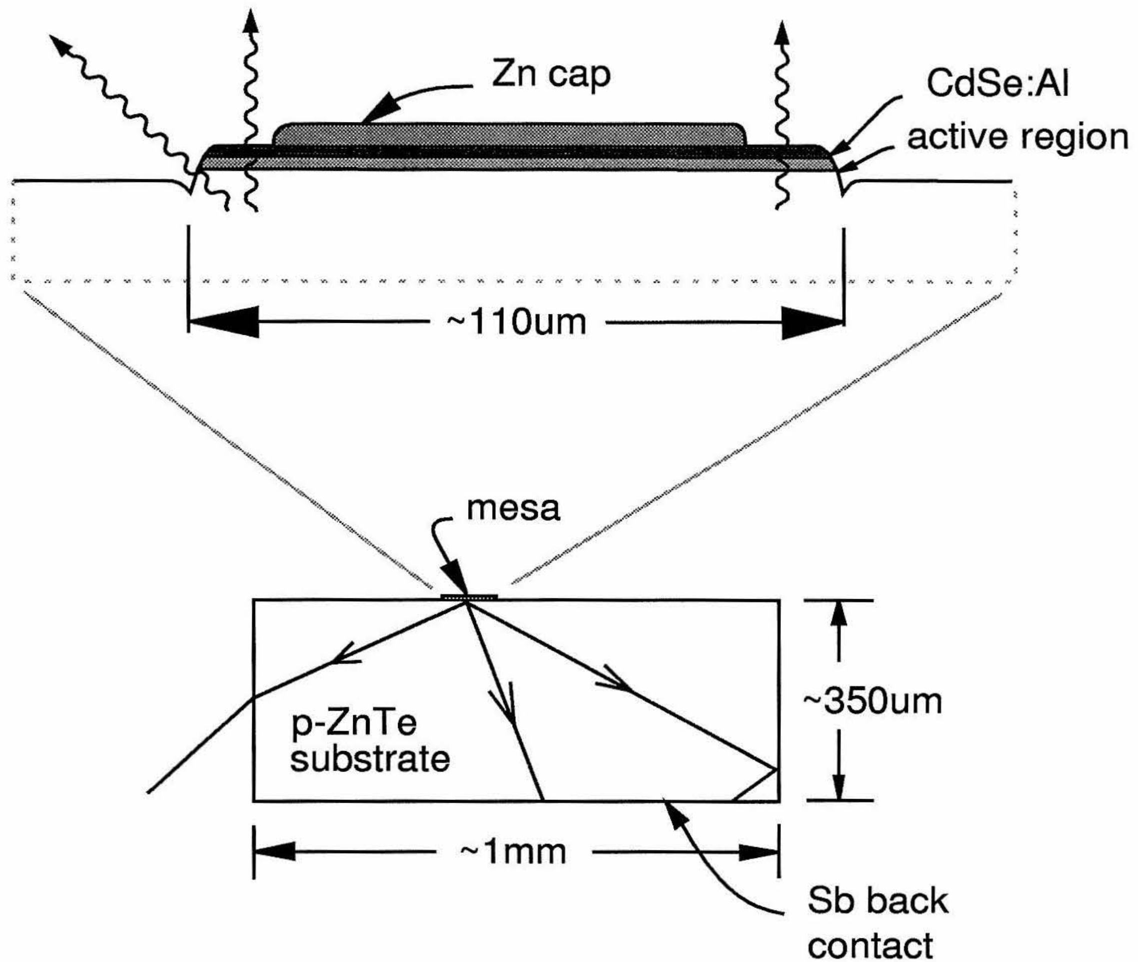

Figure 3.8: Sketch of a simple mesa diode fabricated from the structure in Figure 3.7. The sample was cleaved into ≈ 1 mm × 1 mm chips for photolithography, then the mesa was isolated by etching through the Zn cap and *n*-CdSe. The Zn cap etched back about 10 μm from the edge of the mesa because Zn etches much faster in the Br_2:ethylene glycol etch than does the semiconductor. Most of the light is absorbed in the Zn cap or at the back contact.

in Figure 3.11. Second, this device was grown without a *p*-type dopant for ZnTe, so we had to rely on the *p*-typeness of the substrate and grow only a thin buffer layer. The slower-than-expected turn-on of our device is probably due to charging of traps in the undoped buffer and possibly also in the $Mg_xCd_{1-x}Se$ which we have still not adequately characterized. In spite of the low carrier concentration of the ZnTe substrate, satisfactory ohmic contacts can be made by evaporating Sb or flash-evaporating Sb_2Te_3, sometimes followed by an anneal at 230°C. It seems likely that this produces high doping in a very thin layer at the contacting surface.

The electroluminescence spectrum in Figure 3.12 shows that we are obtaining electron injection into the ZnTe. The large peak is band-edge emission from ZnTe. The calculated carrier densities in Figure 3.5 show the density of injected electrons extending past the thin buffer layer into the substrate; in fact, nearly all of the recombination occurs in the substrate, which is of poor structural quality and contains an isoelectronic oxygen recombination center. The weaker signal in the red in Figure 3.12 is from this recombination center in the substrate. We never observe any luminescence from the CdSe, indicating that the graded injector is blocking holes as desired.

The emission around the edge of the mesa is quite intense, though the total light output is small since light can escape from only a small region of the device. The poor light extraction efficiency is not a fundamental problem. For instance, the Zn cap could be replaced with a transparent conductor such as In_2O_3:Sn (ITO), which has been used to contact *n*-type ZnSe:Cl for LEDs [7]. Commercial LEDs are thinned and cleaved into cubes about 250 μm on a side. The sides are roughened to reduce internal reflection, and then the cube is placed in a reflective metal cup, wire bonded, and encased in epoxy resin with an index of refraction chosen to minimize losses due to internal reflection, as shown on the left side of Figure 3.13. The same steps could be taken to improve the efficiency of the graded-$Mg_xCd_{1-x}Se$ LEDs, as shown on the right side of Figure 3.13. We can currently fabricate our devices into cubes, but the doping of our ZnTe substrate is too low to make the

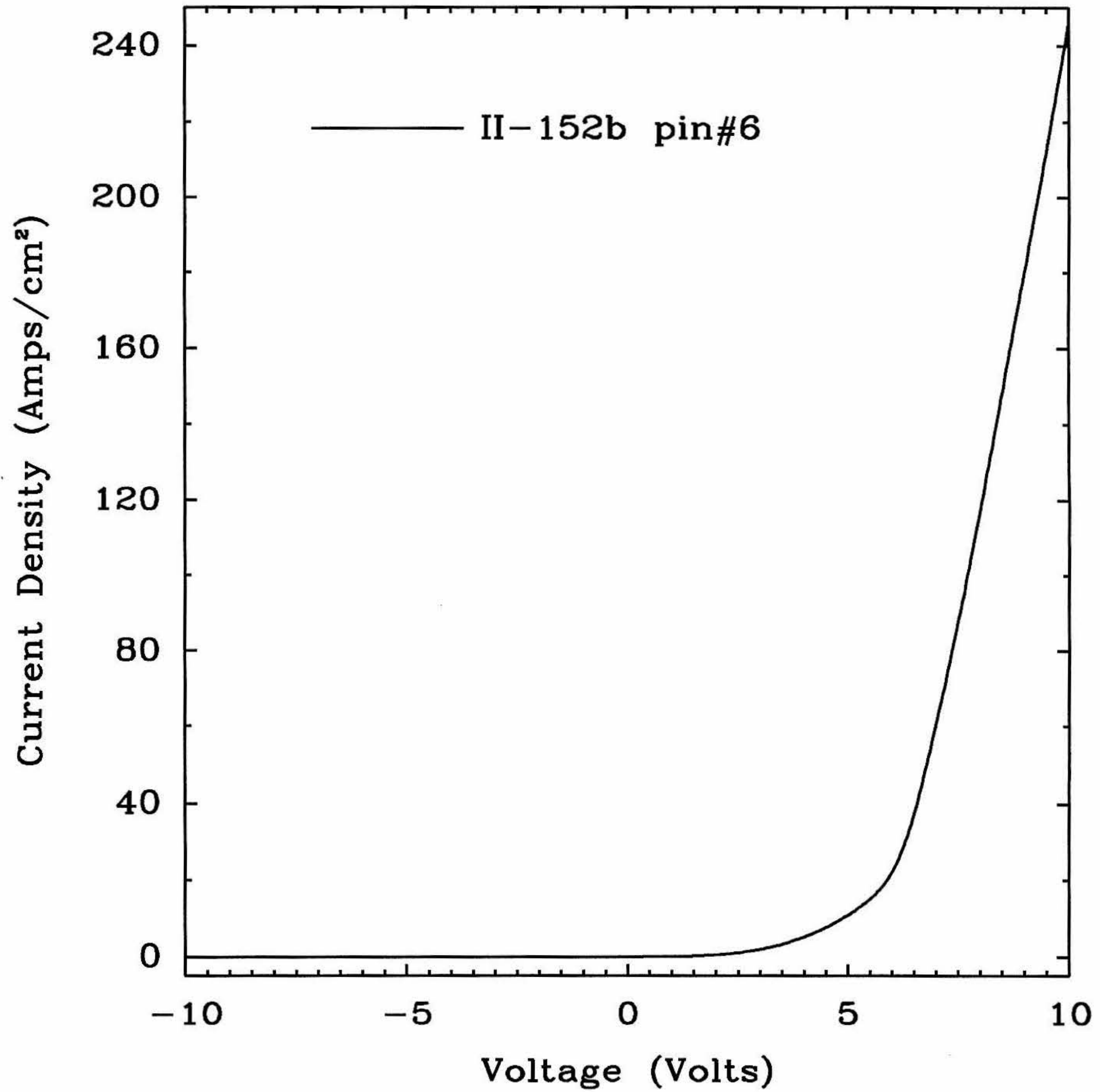

Figure 3.9: Current density vs. voltage at room temperature for device II-152b, the graded $Mg_xCd_{1-x}Se$ LED described in Figures 3.7 and 3.8.

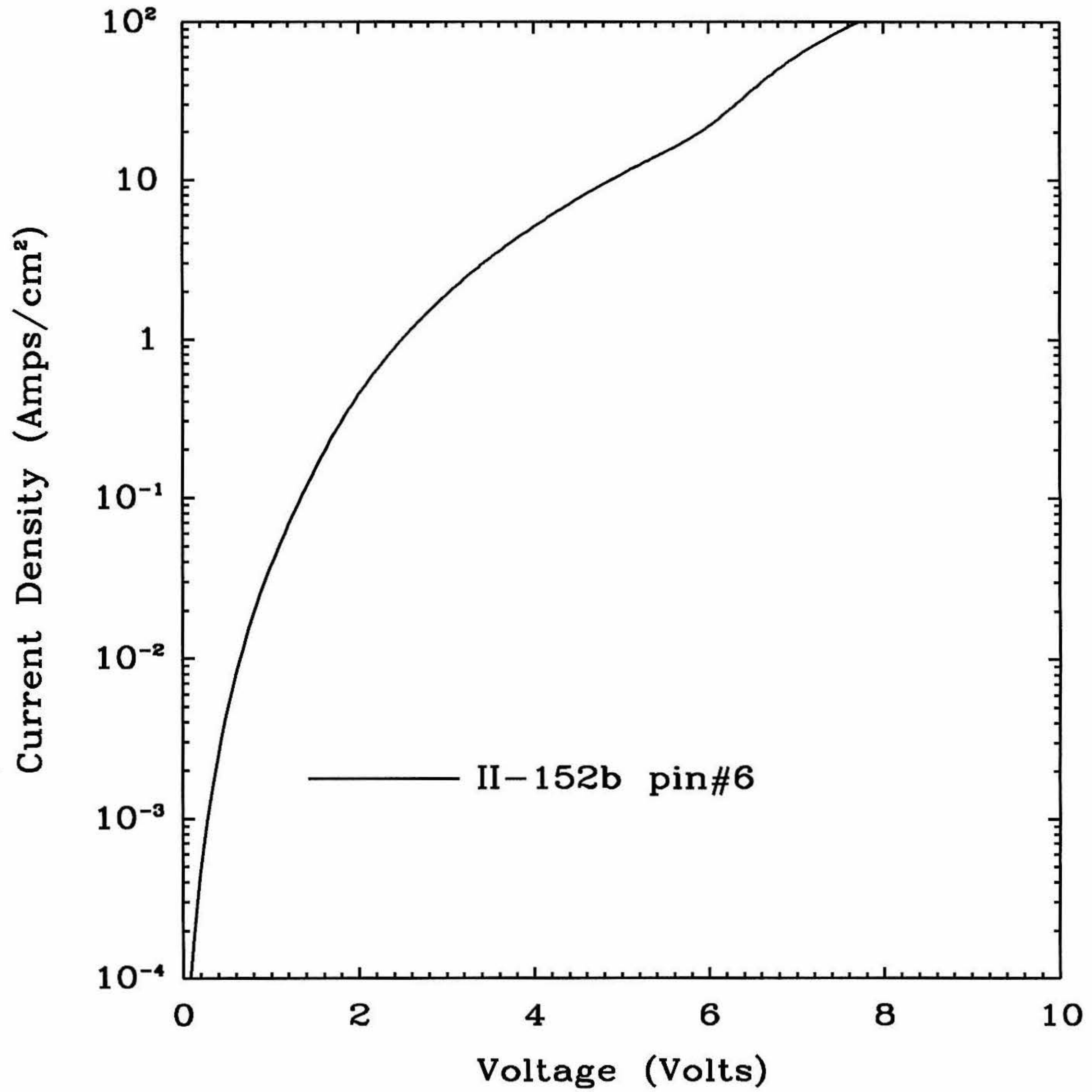

Figure 3.10: Log plot of current density vs. voltage at room temperature for device II-152b, the graded $Mg_xCd_{1-x}Se$ LED described in Figures 3.7 and 3.8.

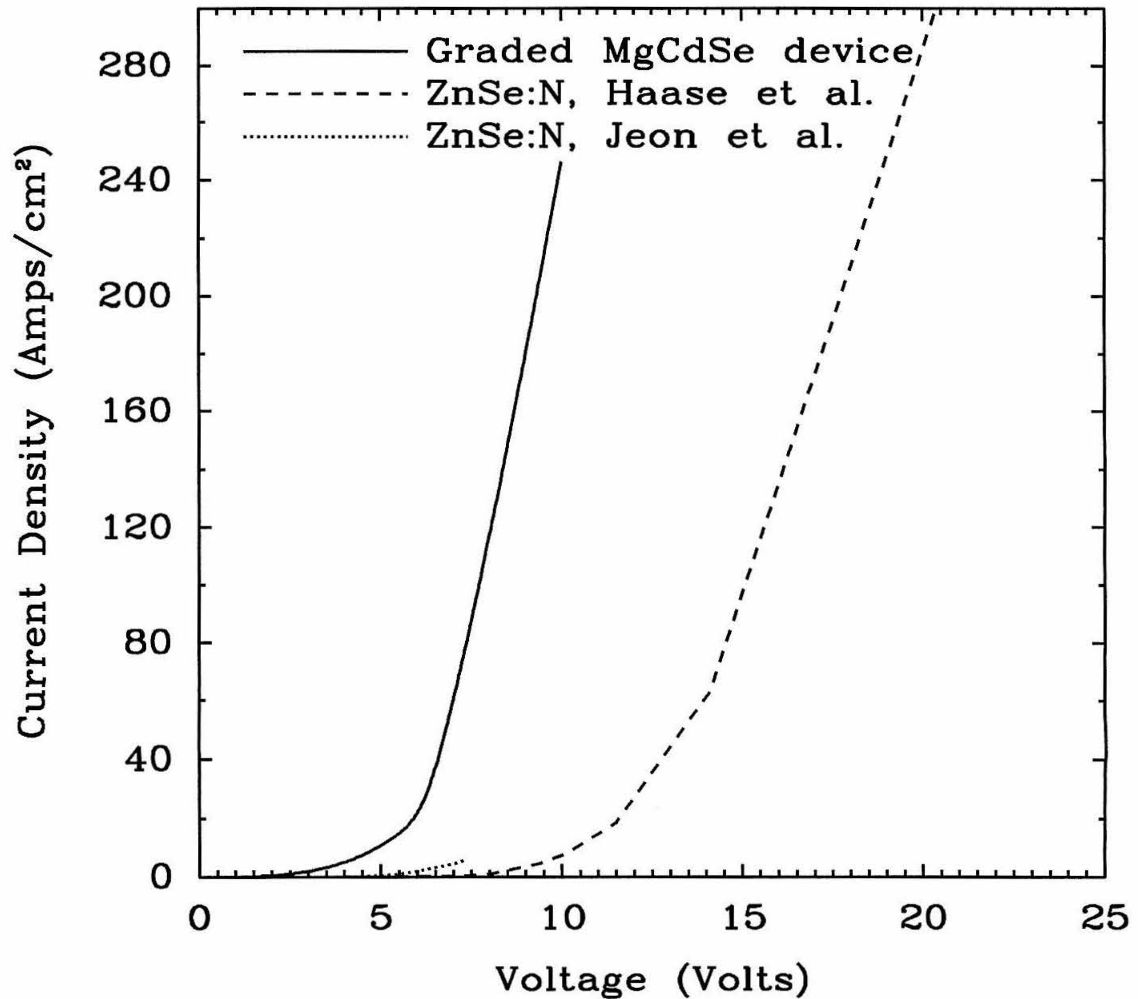

Figure 3.11: *J-V* characteristics of device II-152b, the graded $Mg_xCd_{1-x}Se$ device described in Figures 3.7 and 3.8, compared to a ZnSe:N laser diode(pulsed)[5] and a ZnSe:N LED[6].

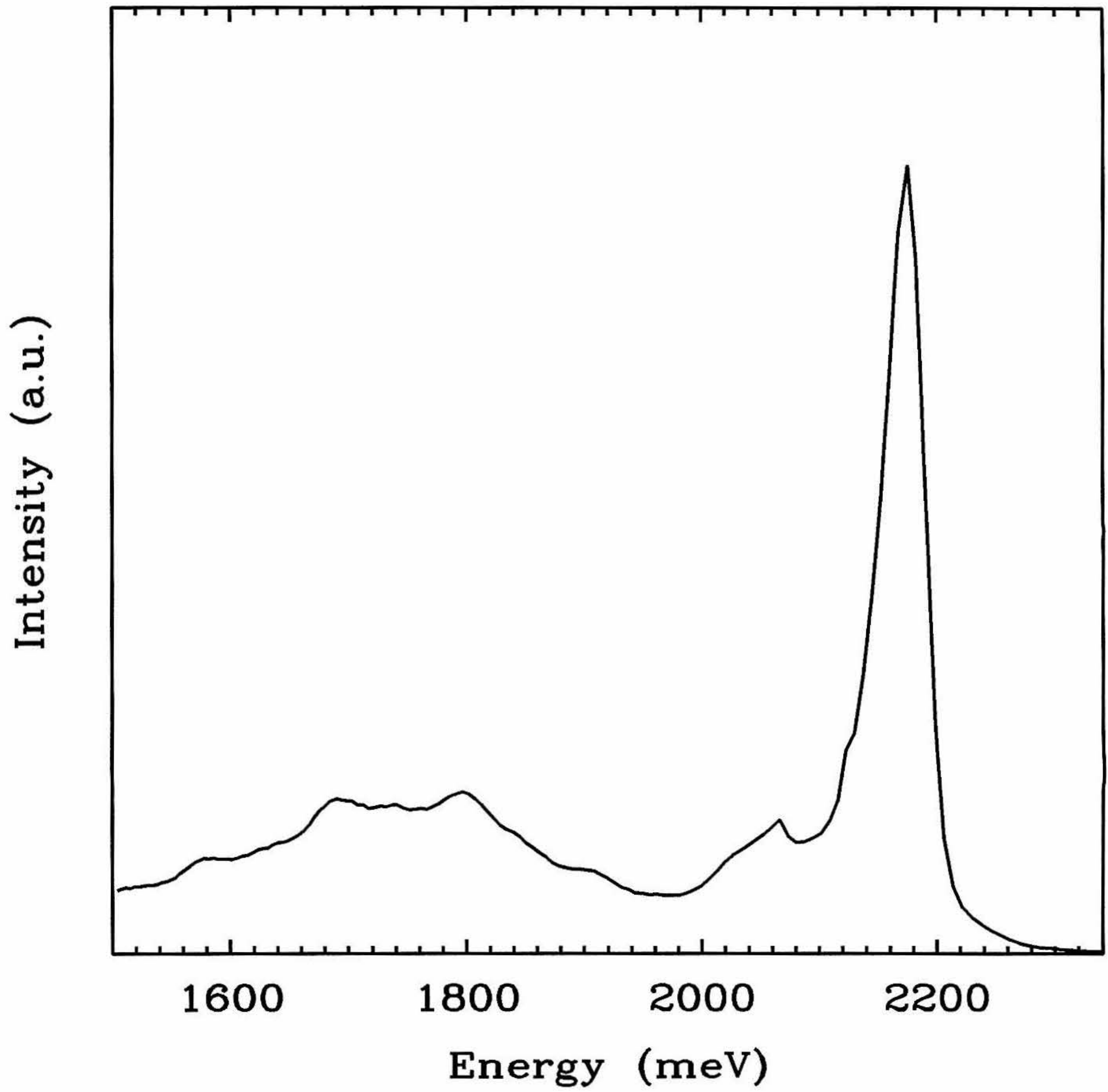

Figure 3.12: Room-temperature electroluminescence spectrum of device II-152b, the graded-$Mg_xCd_{1-x}Se$ LED described in Figures 3.7 and 3.8. The broad peak centered around 1.8 eV is from an impurity center present in the substrate.

small-area ohmic contact required in these devices. We have not put extensive effort into improving the light extraction in these devices because the main reason for fabricating them was to demonstrate graded injection in the simplest structure possible before moving on to blue LEDs and green and blue lasers, which are technologically more interesting.

3.2.2 *p*-type doping of ZnTe

The lack of a good *p*-type dopant for MBE of ZnTe was a serious limitation on the device structures we were able to fabricate. For the green LED, we relied on the *p*-typeness of the ZnTe substrate for the *p* region of the device. This results in an unacceptably high operating voltage and in poor radiative efficiency, since the electrons are injected into the bulk substrate where many of them recombine non-radiatively at defects. For laser diodes or efficient LEDs we need to be able to grow thick *p*-type buffer layers.

The difficulty of doping ZnTe *p*-type during MBE growth was unexpected and somewhat ironic, since one of the reasons we chose to work with ZnTe was its natural tendency to be *p*-type. When ZnTe is grown by bulk crystal growth techniques, a slight excess of Te will produce *p*-type material because Zn vacancies act as double acceptors. During MBE growth, excess Zn or Te can re-evaporate from the surface, resulting in stoichiometric crystals with high resistivity.

We tried doping the ZnTe with Sb from an effusion cell, but Sb evaporates as Sb_2 and Sb_4 molecules. The dimer in particular is tightly bound, and it is highly improbably that this molecule will dissociate during growth at 300°C. For reasonable doping fluxes, very little Sb incorporates in the growing crystal. At high doping fluxes, some Sb will incorporate, but this produces only slight *p*-typeness and poor crystal quality. We attempted to crack the Sb down to monomers by running a cracking cell at 1300°C, and this greatly improved the incorporation of Sb, but the Sb seemed to interfere with the growth of the ZnTe.

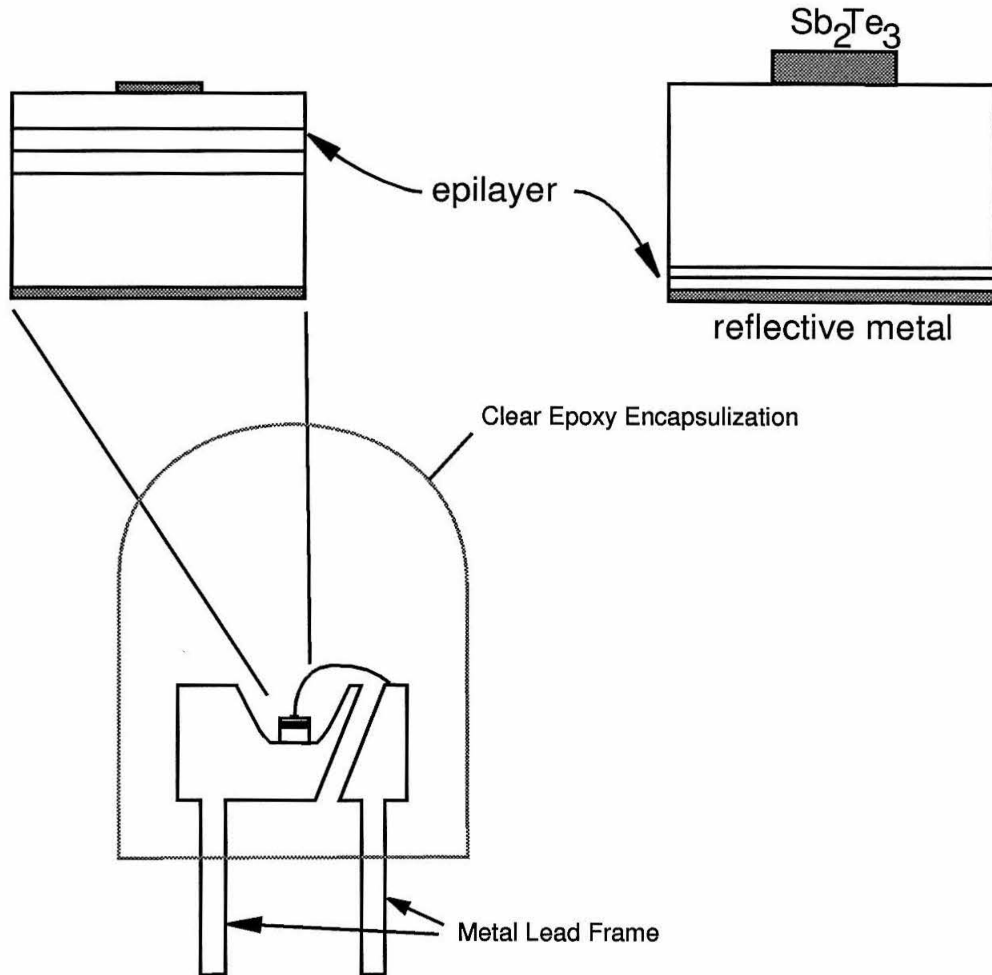

Figure 3.13: Device structures to improve LED efficiency. Left: Commercial LED package (After Kuo [8]). Device is cleaved into a cube roughly 250 μm on a side, placed in a reflective cup, wire bonded, and encased in epoxy with an index of refraction chosen to minimize internal reflection. Right: The graded-$Mg_xCd_{1-x}Se$ green LEDs could be put in these packages if the carrier concentration of the ZnTe substrate were high enough to allow a small area ohmic contact. If ITO were used to contact the epilayer, the device could be packaged with the epilayer on top, as in the commercial LED.

The best dopant which has been found for p-type doping of ZnTe during MBE growth is N from the N-plasma sources used for p-type doping of ZnSe [9]. In ZnSe, N doping will not produce net acceptor concentrations above 2×10^{18} /cm^3, and the doping may not be stable. We recently installed a N-plasma source on our MBE machine, and have measured free-hole concentrations in ZnTe exceeding 1×10^{20} /cm^3. There are no signs of instability, and the incorporation and doping efficiency seem to be much higher in ZnTe than in ZnSe. In fact, we are having trouble obtaining sufficiently *low* doping levels. The orifice plate in the plasma source was designed for ZnSe doping, and at the minimum sustainable RF power and N flow rate we obtain doping in excess of 10^{19}/cm^3. Such high doping levels result in poor luminescence, and it may be necessary to vent the MBE chamber to insert a more restrictive orifice plate.

3.3 Conclusions

We have proposed a new device structure, the graded injector, for short-wavelength light emitters, and fabricated LED structures to demonstrate the validity of the idea. Chapter 4 discusses some of the difficulties which were encountered in growing and fabricating the devices. One difficulty, the lack of a p-type dopant for MBE growth of ZnTe, was a serious limitation thoughout most of this research, but we have recently added a N-plasma source which is proving to be very effective.

With p-type doping from the N-plasma source, we should be able to fabricate green LEDs with normal diode characteristics. Then we can move on to more complicated structures such as blue LEDS and green and blue laser diodes. Since the N-plasma is such an effective dopant for ZnTe, we should be able to maintain p-type doping as we open up the bandgap of the ZnTe with Mg to make blue devices.

Bibliography

[1] M. W. Wang, M. C. Phillips, J. F. Swenberg, E. T. Yu, J. O. McCaldin and T. C. McGill, to be published in *Journal of Applied Physics*, May, 1993.

[2] J. O. McCaldin, T. C. McGill and C. A. Mead, *Phys. Rev. Lett.* **36**, 56 (1976).

[3] H. Okuyama, K. Nakano, T. Miyajima and K. Akimoto, *Jpn. J. Appl. Phys.* **30**, L1620 (1991).

[4] M. C. Phillips, M. W. Wang, J. F. Swenberg, J. O. McCaldin and T. C. McGill, *Appl. Phys. Lett.* **61**, 1962 (1992).

[5] M. A. Haase, J. Qiu, J. M. Depuydt, and H. Cheng, *Appl. Phys. Lett.* **59**, 1272 (1991).

[6] H. Jeon, J. Ding, A. V. Nurmikko, W. Xie, M. Kobayashi, and R. L. Gunshor, *Appl. Phys. Lett.* **60**, 892 (1992).

[7] M. Hagerott, H. Jeon, A. V. Nurmikko, W. Xie, D. C. Grillo, M. Kobayashi and R. L. Gunshor, *Appl. Phys. Lett.* **60**, 2825 (1992).

[8] C. P. Kuo, R. M. Fletcher, T. D. Osentowski, M. C. Lardizabal, M. G. Craford and V. M. Robbins, *Appl. Phys. Lett.* **57**, 2937 (1990).

[9] J. Han, T. S. Stavrinides, M. Kobayashi, R. L. Gunshor, M. M. Hagerott and A. V. Nurmikko, *Appl. Phys. Lett.* **62**, 840 (1993).

Chapter 4

MBE growth of II-VI Compounds

4.1 Introduction

Yao [1] gives an extensive discussion of the growth of II-VI compounds by MBE and a review of work up to the early 1980s. This chapter will discuss some of the details of the growth and fabrication of devices from II-VI semiconductor compounds, emphasizing differences from standard III-V and Si practice.

4.2 Growth

4.2.1 Substrate choice

One difference between III-V and II-VI MBE is the availability of substrates. Many III-V compounds are available as large, single-crystal, oriented substrates, but very few II-VI substrates are sold commercially. CdTe and $Cd_xZn_{1-x}Te$ with a few percent Zn are sold for $Hg_xCd_{1-x}Te$ IR detector growth, but the lattice constant of these substrates is too large to be useful for ZnSe- or ZnTe-based systems.

GaAs

Since the lattice constant of GaAs is only 0.26% less than that of ZnSe, and since GaAs substrates are relatively inexpensive and available in a variety of sizes and conductivity types, most II-VI MBE is done on GaAs substrates. Often dual-chamber MBE systems are used, so that the GaAs substrate can be deoxidized and a buffer layer grown in the III-V chamber before moving through UHV to the II-VI chamber. The conduction band of ZnSe lies above the conduction band of GaAs, but the offset is small enough[1] to allow an n-type back contact through an n-GaAs substrate. Semi-insulating GaAs substrates simplify the study of doped epilayers by Hall-effect measurements.

ZnTe is often grown on GaAs in spite of a 7% lattice mismatch. This severe mismatch can be improved upon somewhat by growing GaSb or InAs buffers on short-period InGaAs-GaAs or GaSb-GaAs superlattices. InAs and GaSb lattice-match more closely to ZnTe, and short-period superlattices bend out dislocations, reducing the number of dislocations threading up into the final epilayer.

GaSb

GaSb is a close lattice match to ZnTe (0.15%), but these substrates are expensive and of lower structural quality than GaAs substrates. Furthermore most researchers do not have dual-chamber MBEs with antimonide growth capability. Our study of $ZnSe_xTe_{1-x}$ epilayers and superlattices was the first reported use of GaSb substrates for MBE growth of II-VIs [6]. We make use of GaSb substrates whenever possible, but the valence band of ZnTe is 0.60 eV lower than that of GaSb [7], making a p-type back contact difficult. Now that we can dope ZnTe heavily p-type with N we should be able to grow on GaSb and make the "back"

[1]Probably 0.2–0.3 eV. The experimental values fall over a wider range [2], probably due to substantial reaction between Ga and Se at the interface, particularly in older measurements. Nearly all ZnSe laser diodes make a back contact through an n-GaAs substrate, and there is very little voltage drop at the n-ZnSe/n-GaAs interface.

contact laterally through a thick *p*-type epilayer. Semi-insulating GaSb substrates are not available, which makes Hall-effect measurements epilayers difficult.

InAs

The lattice constant of InAs is about 0.75% smaller than that of ZnTe, so the lattice match is not as good as for GaSb, but the valence-band offset between ZnTe and InAs is quite small. This offset has not been directly measured, but from the measured ZnTe/GaSb and GaSb/InAs offsets [2] we can estimate that the valence band of ZnTe lies less than 0.1 eV below that of InAs. Thus it should be possible to make a *p*-type back contact for a ZnTe device through an InAs substrate. InAs substrates are available, but our III-V chamber does not have a *p*-type dopant for InAs.

Substrate-ion out-diffusion

Since group III and group V elements are dopants in II-VI materials, III-Vs are not ideal substrates for II-VI growth. Some group III and group V ions are incorporated in the II-VI epilayer, and they show up in the optical and electrical characteristics of the epilayers. Even when the III-V/II-VI interfaces are quite abrupt, group III and group V ions are often found at the surface of thick II-VI epilayers grown on III-V substrates.

There is evidence that dislocations provide a path for the diffusion of substrate ions through the epilayer. Figures 4.1 and 4.2 show the effects of lattice match on the impurity peaks in the PL. Figure 4.1 shows PL spectra from ZnTe epilayers on three different III-V buffers on GaAs substrates and a ZnTe epilayer on a polycrystalline ZnTe substrate. The second and third samples contain short-period superlattices to reduce the number of misfit dislocations extending into the GaSb and InAs buffers. The intensity of luminescence under identical pumping conditions increased with better lattice-matching of the buffer layer to ZnTe. The

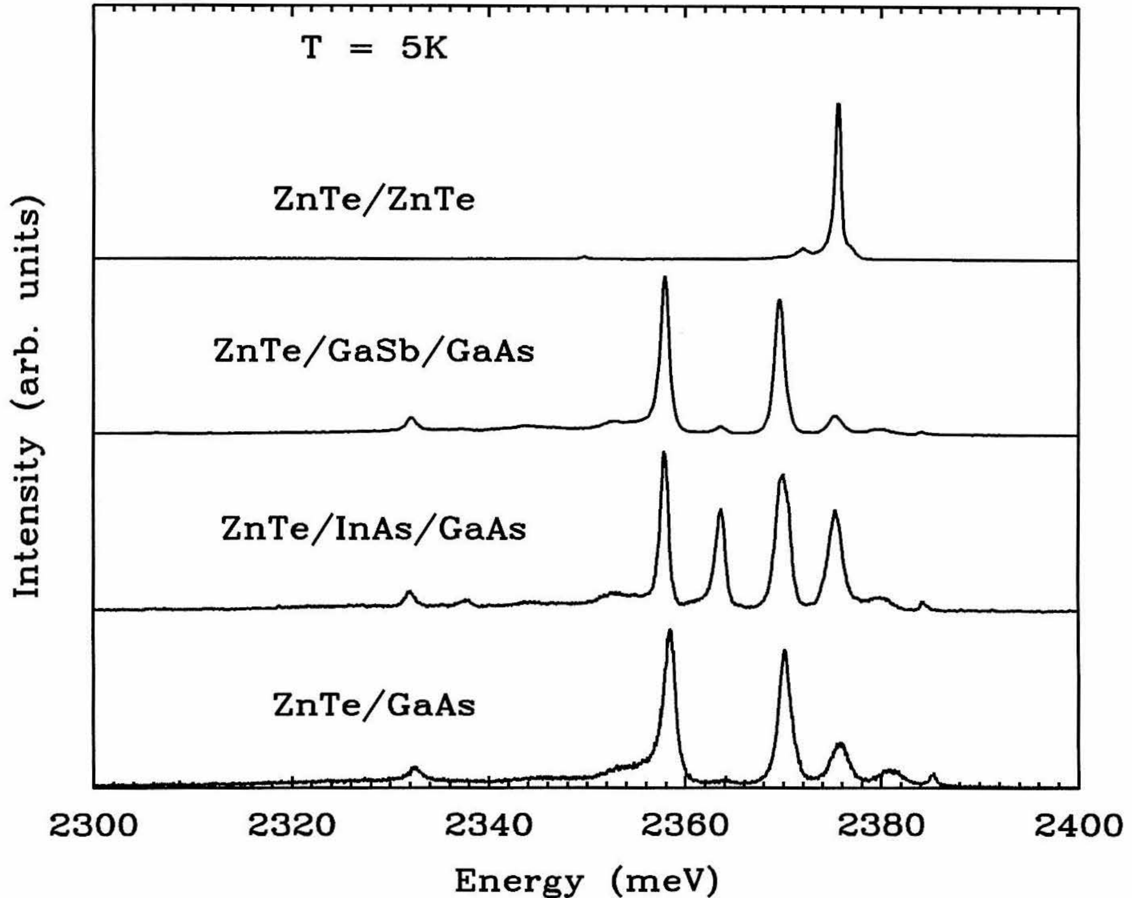

Figure 4.1: Photoluminescence from ZnTe epilayers on a polycrystalline ZnTe substrate and on three different III-V buffers on GaAs substrates [3].

spectrum from ZnTe on polycrystalline ZnTe is dominated by one strong peak; starting with a GaAs substrate always yields spectra with several large peaks, some of which seem correlated to the presence or absence of particular elements in the III-V buffers. Indeed, Rajakarunanayake *et al.* [3] found group III and group V impurities in these epilayers using secondary ion mass spectroscopy.

Figure 4.2 shows PL from ZnTe on a GaSb buffer on a GaSb substrate, and compares it to PL from ZnTe on ZnTe and ZnTe on a GaSb buffer on a GaAs substrate. The spectrum from ZnTe on a GaSb substrate is dominated by one

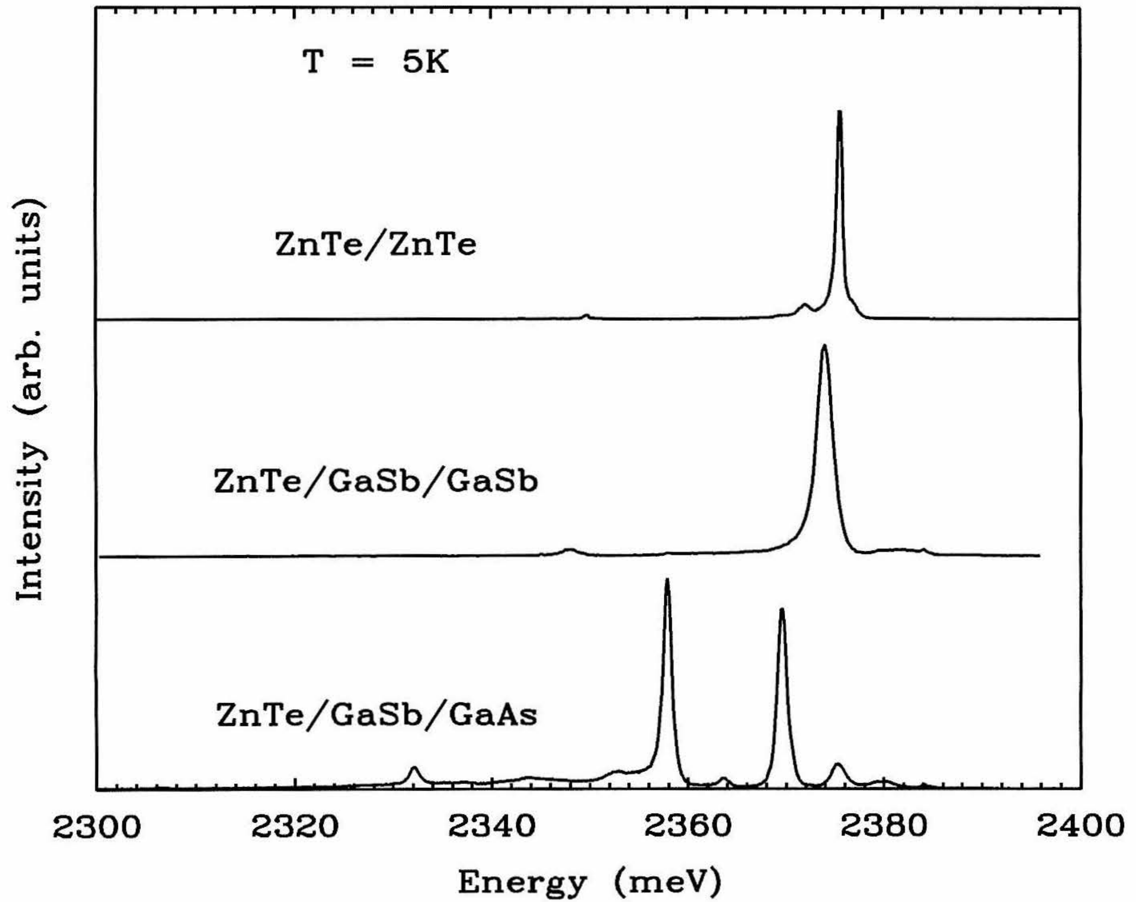

Figure 4.2: Photoluminescence from ZnTe epilayers on a polycrystalline ZnTe substrate, on a GaSb buffer on a GaSb substrate and on a GaSb buffer on a GaAs substrate [4]

large peak, perhaps shifted by strain and broadened by non-uniform strain since this layer was near the critical thickness for ZnTe on GaSb. The absence of multiple peaks may indicate that the improved lattice match has reduced diffusion of substrate elements along dislocations.

ZnTe

If high-quality ZnTe substrates were available, they would be preferable in most cases to heteroepitaxy on III-V substrates because homoepitaxy gives perfect lattice match and freedom from contamination by substrate ions, but the only source of ZnTe substrates is custom growths.

Our first graded-$Mg_xCd_{1-x}Se$ devices were grown on polycrystalline substrates grown from a ZnTe melt. With polycrystalline substrates we could not control the orientation of the growth, and the reflection high-energy electron diffraction which is normally used to monitor the crystal growth during MBE was nearly useless. Polycrystalline substrates also break easily along crystal boundaries, making them difficult to handle or cleave into regular dice. These substrates were grown Te rich to make them p-type, but many regions were nearly opaque with Te precipitates.

We obtained our first single-crystal ZnTe substrates from Eagle-Picher [5]. They use physical-vapor-transport growth with a proprietary seeding process which seeds a single crystal across a 2 inch substrate. Crystal quality varied between boules, with some boules turning out polycrystalline. Undoped boules were p-type with resistivities of 5–10 Ω cm. One attempt to dope with Sb resulted in a boule with resistivity of 1.3 Ω cm, and this boule was used for most of the graded-$Mg_xCd_{1-x}Se$ LEDs. All subsequent attempts at doping with Sb, and one attempt to dope with Na, have resulted in polycrystalline boules.

4.2.2 Substrate preparation and deoxidation

An important difference between III-V MBE growth and II-VI MBE growth can be illustrated by contrasting the growth of ZnTe on a ZnTe substrate using elemental Zn and Te sources with the growth of GaAs on a GaAs substrate using elemental Ga and As sources. For typical ZnTe growth, the ZnTe substrate might be held at 330 °C, with the Zn and Te at 280 °C and 320 °C, respectively. Since the substrate temperature is near or above the source temperatures, excess Zn or Te will re-evaporate from the surface. For GaAs, the substrate might be held around 600 °C, with the Ga and As at 960 °C and 300 °C. Excess As will evaporate from the GaAs surface, but Ga will collect and eventually form puddles.

At normal growth temperatures, the ZnTe surface is stable, and if heated above normal growth temperatures the Zn and Te will begin evaporating congruently, slowly roughening the surface. At normal GaAs growth temperatures the As will evaporate incongruently, leaving behind puddles of Ga. If enough As flux is supplied to keep the surface As rich, the GaAs surface is stable well above the growth temperature. This is important for preparing GaAs substrates for growth. When a GaAs substrate is loaded into vacuum, oxide on the surface can be removed by heating under an As flux, since the oxide evaporates before Ga.

In the case of ZnTe, the surface cannot be stabilized with a Zn or Te flux. As the substrate is heated above growth temperature, Zn and Te will evaporate more rapidly than O bound to Zn. This will eventually roughen the surface without removing all of the oxide. Since our II-VI MBE system is a slightly modified III-V MBE system, we have no other provision for oxide removal. Residual oxide on the ZnTe surface nucleates twins in the growing crystal. The best solution we could find was to first heat the ZnTe substrates to 460 °C for 10–15 min, then move them into the XPS analysis chamber. XPS shows that the initial heating removes O bound to Te, but not the O bound to Zn. The analysis chamber has limited Ar ion sputtering capabilities, which we use to sputter the remaining O from the

surface. The sputtering damages the ZnTe surface, so we anneal the substrates at 460 °C in the MBE chamber before growth.

In the long run it may be necessary to add a cleaning module—perhaps containing an electron-cyclotron-resonance plasma source—to do the cleaning faster and with less damage.

4.2.3 Substrate mounting for growth

III-V substrates are usually mounted for growth by In bonding them to Mo blocks, or by fixing them in special holders made for standard-size substrates. Since II-VI substrates are not available in standard sizes, they cannot be mounted in these holders. The In bonding process results in the formation of a heavy oxide layer, which can be easily removed in the case of III-V materials, as discussed in Section 4.2.2. In the case of II-VI materials, the oxide layer is very difficult to remove. The molten In also tends to creep onto the surface of the substrate during growth.[2]

Our solution is to sand blast a 3 inch Si wafer to leave two thin springs of Si pointing in towards the center of the wafer, and a continuous ring of Si around the circumference. We bond these wafers to the Mo blocks, applying In only around the circumference of the wafer. We then gently lift the thin Si springs and slide the small chips of ZnTe underneath them. The substrate is held down mechanically by the spring, and the In is kept from coming into direct contact with the substrate.

This is only a partial solution. The thermal contact between the block and the substrate is much less reliable than for In bonded samples. At typical growth temperatures of 300 °C there is little radiative heating, so large temperature differences may exist between the substrate and the block. II-VI growth temperatures

[2]This does not generally occur when In-bonded III-V substrates are used for II-VI growth, especially if any excess In is cleaned off the block with a razor blade after bonding. One possible reason for the lack of contamination from In with In-bonded III-V substrates is that the As or Sb flux during the III-V growth probably forms a layer of InAs or InSb over the In, keeping it from creeping.

are too low for the optical pyrometers used to monitor the substrate temperature during III-V growth. One solution would be to use *in situ* PL to monitor the change in bandgap of the substrate with temperature.

Bibliography

[1] T. Yao in *The Technology and Physics of Molecular Beam Epitaxy,* edited by E. H. C. Parker (Plenum, New York, 1985).

[2] E. T. Yu, J. O. McCaldin and T. C. McGill, *Solid State Phys.* **46**, 1 (1992).

[3] Y. Rajakarunanayake, B. H. Cole, J. O. McCaldin, D. H. Chow, J. R. Söderström and T. C. McGill, *Appl. Phys. Lett.* **55**, 1217 (1989).

[4] M. C. Phillips, Y. Rajakarunanayake, J. O. McCaldin, D. H. Chow, D. A. Collins and T. C. McGill, *Proc. SPIE - Int. Soc. Opt. Eng.* **1285**, 152 (1990).

[5] Eagle-Picher Research Laboratory, Miami, Oklahoma.

[6] M. C. Phillips, Y. Rajakarunanayake, J. O. McCaldin, R. H. Miles, D. H. Chow, D. A. Collins and T. C. McGill, *Mat. Res. Soc. Symp. Proc.* **198**, 439 (1990).

[7] E. T. Yu, M. C. Phillips, D. H. Chow, D. A. Collins, M. W. Wang, J. O. McCaldin and T. C. McGill, *Phys. Rev. B* **46**, 13379 (1992).